NEUTRON MULTIPLICITY MONITOR OPERATIONS
AT SEA LEVEL AND 3800 METER ELEVATION

(Covering period June 22, 1965 to June 22, 1966)

Final Report for Contract NASw-1240

R. A. Nobles

R. A. Alber

E. B. Hughes

L. L. Newkirk

G. T. Reynolds

M. Walt

i

PROLOGUE

The Lockheed Neutron Multiplicity Monitor is a unique type cosmic ray neutron monitor, designed for the efficient exploitation of the energy dependence of multiple neutron production to obtain information on the energy spectrum of the incident secondary cosmic radiation. The basic monitor was designed and constructed by Lockheed Missiles and Space Company (LMSC) and has been operated during the past year with support by the National Aeronautics and Space Administration under contract NASw-1240. This is the final report on research work performed under that contract.
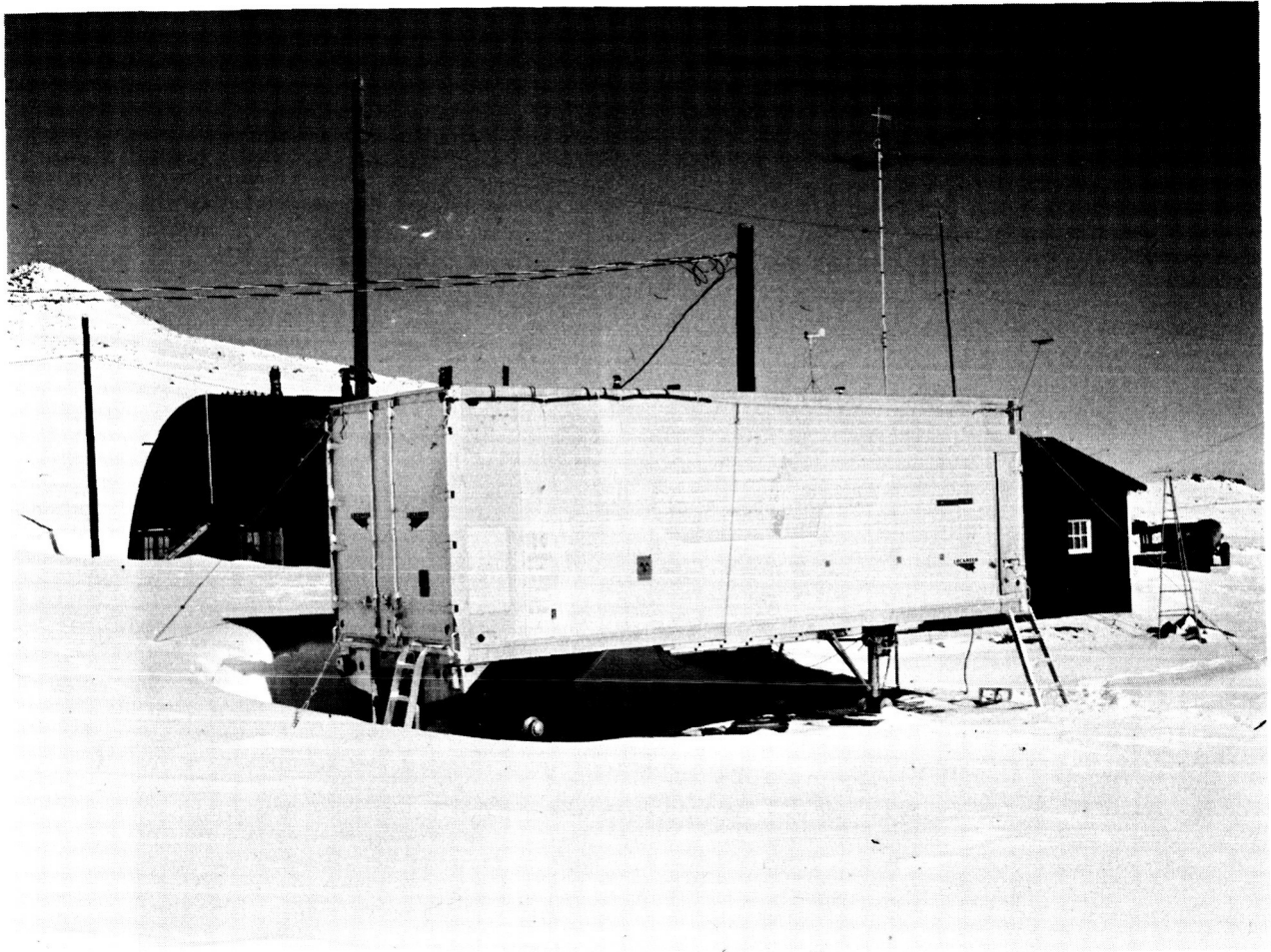
I   INTRODUCTION

The cosmic radiation arriving at the earth varies both in energy spectrum and intensity as a function of time, the largest changes occurring in the low energy portion of the spectrum in the region below 50 BeV.   Long term variations are closely correlated with the general solar 11-year activity cycle and short term variations are correlated with discrete events such as flares and other solar disturbances.   The importance of investigating these energy, intensity, and time variations lies in the information they can provide about the electromagnetic conditions in the earth-sun region and the high energy processes occurring at the sun.   Such studies can provide insight into particle accelerating mechanisms within the solar system and yield information on the structure and turbulence of the magnetic fields within the solar plasma clouds.

Neutron monitors are a type of cosmic ray detector which operate deep in the atmosphere and are especially sensitive to variations in the low energy portion of the primary cosmic ray spectrum.   Such monitors have been operated in many parts of the world for more than a decade.   Because of their high sensitivity, world-wide coverage and continuity of operation, these detectors supply data which is important in its own right and which is complementary to that obtainable from satellite-borne instrumentation.   The literature on the subject is extensive; the following are a few of the principle papers and review articles; Simpson (1953, 1964), Webber (1962), Lockwood (1962), McCracken (1962) and Carmichael (1962).

Simpson-type neutron monitors made important contributions to the success of the International Geophysical Year , 1957-58, and an improved higher counting rate version of the monitor was developed by Carmichael (1964A) for use during the International Quiet Sun Year, 1964-65.

Neutron monitors respond principally to high energy secondary nucleons produced by the interaction of primary co'smic radiation with the atmosphere. These secondary nucleons penetrate deep into the atmosphere and interact with nuclei in the heavy target of the monitor, producing a number of low energy (few MeV) neutrons in the process. These low energy neutrons are thermalized by a moderator and detected by BF_3 filled proportional counters. The ordinary neutron monitor is essentially an intensity measuring device, energy spectrum information being obtained by the correlation of the response of a number of monitors located at positions which have different geomagnetic cut-off energies.

The LMSC monitor is unique in that it gives intensity information similar to an ordinary monitor and, in addition, yields information on energy spectrum variations. This is accomplished by observing the multiplicity with which the low energy neutrons are produced in the target. The multiplicity, i. e. , the average number of neutrons per event, increases with the energy of the producing radiation; hence variations of this parameter are related to the energy spectrum of the primary radiation (Hughes 1961). Measurement of multiplicity offers the possibility of observing spectrum changes at energies greater than the equatorial geomagnetic cut-off energy. Furthermore, the interpretation of spectral changes observed during magnetic storms is not sensitive to storm-time geomagnetic cut-off uncertainties.

The LMSC monitor differs from the ordinary monitor in several important respects: first, it has a higher intrinsic efficiency; that is, it counts a larger fraction of the internally produced neutrons, a feature which facilitates multiplicity measurements; second, it has electronic circuitry for multiplicity

measurements; third, its greater target thickness allows operation more nearly as a total energy detector. **As** a consequence of its higher efficiency (from **3** to 8 times that of an ordinary monitor) the LMSC monitor responds to a larger fraction of the very low energy, low multiplicity events. This low energy sensitivity together with the multiplicity measurement capability which, in essence, separates the response into energy intervals greatly increase the sensitivity to the low energy end of the cosmic ray spectrum.

A diagram of the LMSC multiplicity monitor is shown in Figs. 25 and **26** of Appendix A. The target is of bismuth, and the moderator is composed of reactor-grade graphite surrounded by a reflector of paraffin. There are twenty-six, B_{10} enriched, BF_3 proportional counter neutron detectors arrayed in the moderator surrounding the target. The entire monitor is enclosed by layers of cadmium and paraffin to reduce sensitivity to externally produced neutrons. The detector geometry and materials were selected by calculating the detection efficiency for various configurations using the S_n approximation to the solution of the neutron transport equation. Bismuth and graphite were used for the target and moderator rather than the more usually employed lead and paraffin because the lower thermal neutron capture cross-sections of bismuth and graphite reduce losses to parasitic neutron capture.

Pulses from the individual counters are presented to electronic circuitry which forms a gate on the first pulse of an event. The gate length, τ , is of 1000 μsec duration, about **2.** 5 times the mean lifetime of neutrons in the detector. Events are sorted according to the number of counts (i.e. , the observed multiplicity) occurring during the gate interval. Multiplicities up to 400 neutrons per event can be recorded. The multiplicity information is stored in a

magnetic core memory and is read out at appropriate intervals on perforated paper tape. In addition, the total neutron count observed in each half of the monitor, the total number of gates formed, the time, barometric pressure and other housekeeping parameters are also recorded on the tape. The gate rate is presented to a rate meter whose output drives a strip-chart recorder to provide a visual record of the event count rate. The rate meter incorporates alarm circuitry which can be set to sense rapid rate changes and originate a high speed cycling mode for better time resolution during flares and Forbush decreases.

A more detailed description of the monitor is given in Appendix **A.**

11 ENERGY RESPONSE

It has been determined experimentally that the primary cosmic radiation in the region of the earth **is** composed of positive nuclei, of which 80-85 percent are protons, 14-19 percent are alphas, and a small percentage are heavier nuclei. An approximate per nucleon differential rigidity spectrum of this radiation is given by

$$J(P) = KP^{-\gamma}$$

where **P** is rigidity in BV, $\gamma \sim$ 2.5, for $2 \leq P \leq 50$ BV and $K \sim 4000$ particles $/m^2/sec/sr.$ Both the intensity and the shape of this spectrum is known to vary with time. One of the principal objectives of investigation is the study of these variations and their correlation and interpretation with respect to astrophysical phenomena.

The primary radiation interacts with nuclei in the atmosphere producing secondary radiations, one component of which is high energy neutrons and

protons. It is these secondary radiations which produce the multiple low energy neutrons within the target to which the multiplicity monitor responds. The exact relationship between the primary radiation and the secondary radiation deep in the atmosphere is not well known since the necessary knowledge of nucleon-nucleus interaction cross-sections is at present not available. Nevertheless, the general features of the relationship are reasonably well established. It is known, for instance, that in a collision of a high energy nucleon with a nucleus the inelasticity of the interaction is, on the average, equal to about 0.5 with most of the energy carried away by a single secondary nucleon. Consequently, the secondary spectrum retains approximately the same shape as the primary spectrum. It follows, then, that with a knowledge of the response of the multiplicity monitor to these Secondary nucleonic radiations information can be obtained on the intensity and spectrum changes of the primary radiation.

The response of the monitor to the nucleonic portion of the secondary radiation can be analyzed as follows:

$$r_m = \int_0^\infty N(E)dE \quad P(E) \quad A\Sigma_{\nu=m} \Sigma_{k=m} [I(E,\nu) \, B(k,\nu) \, B(m,k)] \tag{1}$$

where r_m is the rate of detection of events with multiplicity m, $N(E)$ is the incident nucleon flux, $P(E)$ is the probability that a nucleon will interact to produce neutrons in the target, A is the effective detection area of the monitor target, $I(E, \nu)$ is the probability that an interacting particle of energy E will produce ν neutrons, $B(k,\nu)$ is the probability that k of the ν neutrons produced will be detected, and $B(m,k)$ is the probability that m of the k detected neutrons will fall within the gate period τ .

$P(E)$ is calculated assuming that the interaction cross-section of a nucleon with bismuth is geometrical (i.e., $1.53 \times 10^{-24} cm2$). $B(k, \nu)$ obeys the binominal distribution:

$$B(k, \nu) = \binom{\nu}{k} \epsilon^k (1-\epsilon)^{\nu-k} \quad , \quad \nu \geq k$$

Averaged over the target volume ϵ was found to have a value of 0.17 for RaBe neutrons. Since the pulse which opens the gate is always counted, $B(m, k)$ is given by

$$B(m, k) = \binom{k-1}{m-1} f^{m-1}(1-f)^{k-m}, \; k \geq m$$

where f is the gate efficiency. For $\tau = 1000$ μsec, f is 0.90 as determined experimentally by observing the exponential time distribution of neutron counts resulting from isolated events.

The function $I(E, \nu)$ contains the essential information relating the neutron multiplicity to the energy of the cosmic ray secondary initiating the event. Knowledge of this quantity is based largely on the work of Hughes (1961) who measured both the average number and the probability distribution of neutrons produced in a standard **IGY** monitor as a function of the energy of the incident nucleons. These basic data were used to calculate the energy dependence of the average number of neutrons produced by incident nucleons on the 450 gm cm^{-2} thick bismuth target of the present monitor. In this calculation, it was assumed that the interaction cross-section was geometrical, that the inelasticity was 0.47, and that after each collision the remaining energy was

carried away by a single nucleon. The result of the calculation, shown in Fig. 1, gives the average number of neutrons produced in the target of the multiplicity monitor by incident neutrons. Because of the cascading effect within the target the average number of neutrons produced is about twice the average number emitted in a single collision of a nucleon with a bismuth nucleus. The function $I(E, \nu)$ was taken to be exponential in ν at all energies, as suggested by the results of Cocconi, et al. (1950), Geiger (1956), and Hughes (1962).

Thus, $I(E, v) = (e^a - 1)e^{a\nu}$ where $\sum\limits_{1}^{\infty} I(E, v) = 1$. The average multiplicity is given by

$$\bar{v} = \Sigma \ v \ (e^a - 1) \ e^{-av} \tag{2}$$

Using the $\bar{\nu}$ versus **E** dependence given in Fig. 1, together with Equation (2), the constant a and hence $I(E, v)$ is established as a function of energy. Since the monitor is triggered by neutrons which may be produced by either charged or neutral incident particles it is not possible to analyze the response in terms of a separate neutron or proton contribution. However, at low energies, where the responses to neutrons and protons are different, the incident flux is predominantly neutrons. At high energies, where the proton and neutron fluxes are comparable, the detector response is identical for both components. Hence, to a good approximation the response can be considered in terms of an effective nucleon spectrum $N(E)$. With the exception of $N(E)$, the incident flux distribution, all quantities in Equation (1) either are measured or can be computed. Hence, $N(E)$ can be determined by adjusting its value to make the computed distribution from Equation (1) fit the observed multiplicity rate distribution.

Fig. 1   The average number of neutrons, $\bar{\nu}$, produced in the target

of the LMSC multiplicity monitor versus the energy of inci-

dent neutrons.
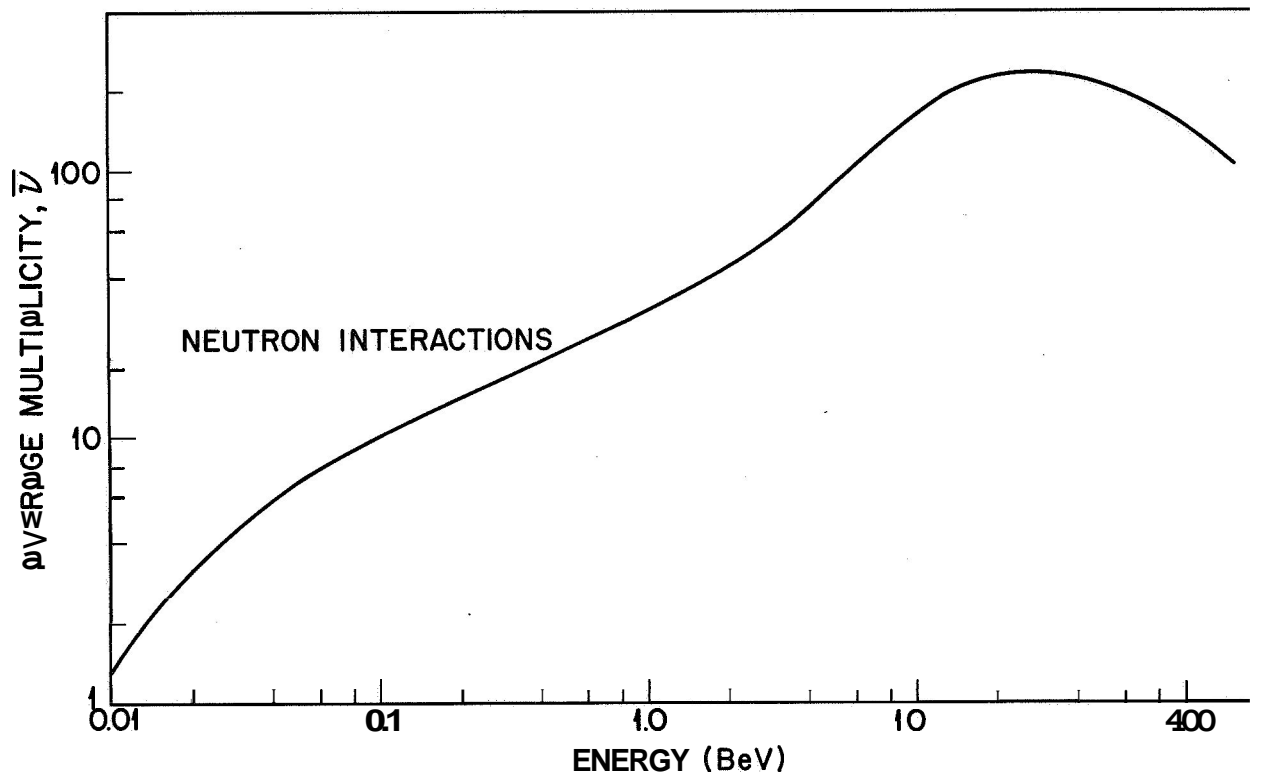
AVERAGE MULTIPLICITY VERSUS ENERGY

Figure 2 gives a family of curves which are characteristic of the response of the multiplicity monitor independent of the incident flux distribution. These curves show the efficiency $k(E,m)$ of each multiplicity channel for the detection of nucleons as a function of nucleon energy. The efficiency is given by the following relationship:

$$k(E,m) = P(E) \sum_{v=m} \sum_{k=m} [I(E,\nu)\ B(k,\nu)\ B(m,k)]$$

and the terms on the right are the same as defined above.

111 MULTIPLICITY OBSERVATIONS

During the period of this contract the monitor was operated at **two** different sites: first, near sea level at Palo Alto, California, **4.7** BV vertical cut-off rigidity, and subsequently at 3800 meter elevation at the University of California's Barcroft Laboratory site on White Mountain, **4.5** BV vertical cut-off rigidity. The monitor operated continuously with a data read-out every hour on the hour. The open circles of Fig. 3 shows typical observed multiplicity distributions R_m, the lower set of points pertaining to sea level data reduced to an atmospheric pressure of 1012 millibars, and the upper set representing 3800 meter data reduced to an atmospheric pressure of **645** millibars. The data presented in the figure are corrected for barometric pressure variations, for background, i.e., neutrons produced outside the Bi target, for instrumental deadtime, for μ-meson capture neutron production, and for overlap of different multiplicity events in a single gate (see Appendix B). Corrections for deadtime and overlap were negligible in the sea level data, and the μ-meson capture effect was insignificant in the mountain data.

Fig. 2   Efficiency of detection of the various multiplicity channels as

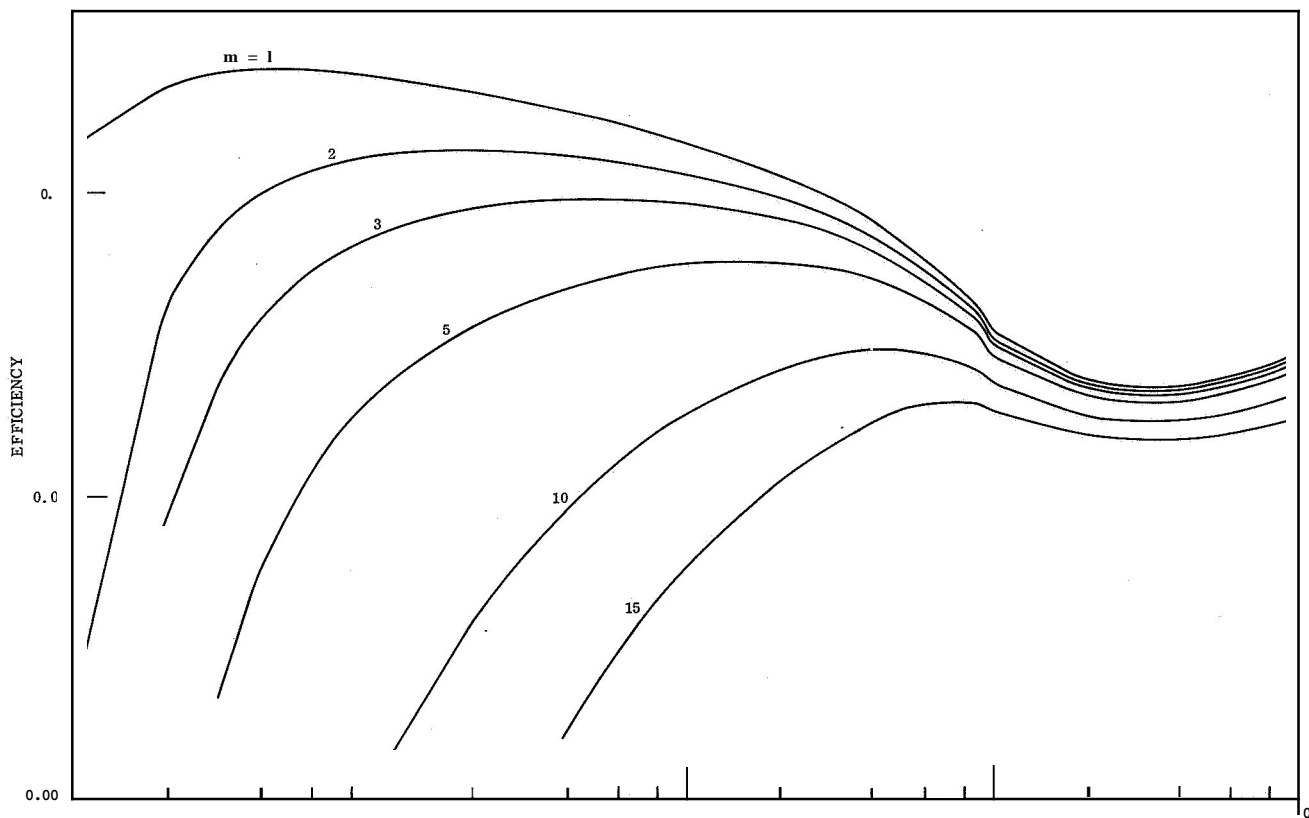a function of incident nucleon energy.

EFFICIENCY

m = 1

2

3

5

10

15

0.

0.0

0.00

Fig. 3   Typical sea level and 3800 meter elevation observed multi-
plicity distribution.   The data points are corrected for atmos-
pheric pressure variations, for background, i.e., neutrons
produced outside the Bi target, for instrumental deadtime,
for μ -meson capture neutron production, and for overlap of
different multiplicity events in a single gate (see Appendix B).
The solid curves are computed multiplicity distributions.
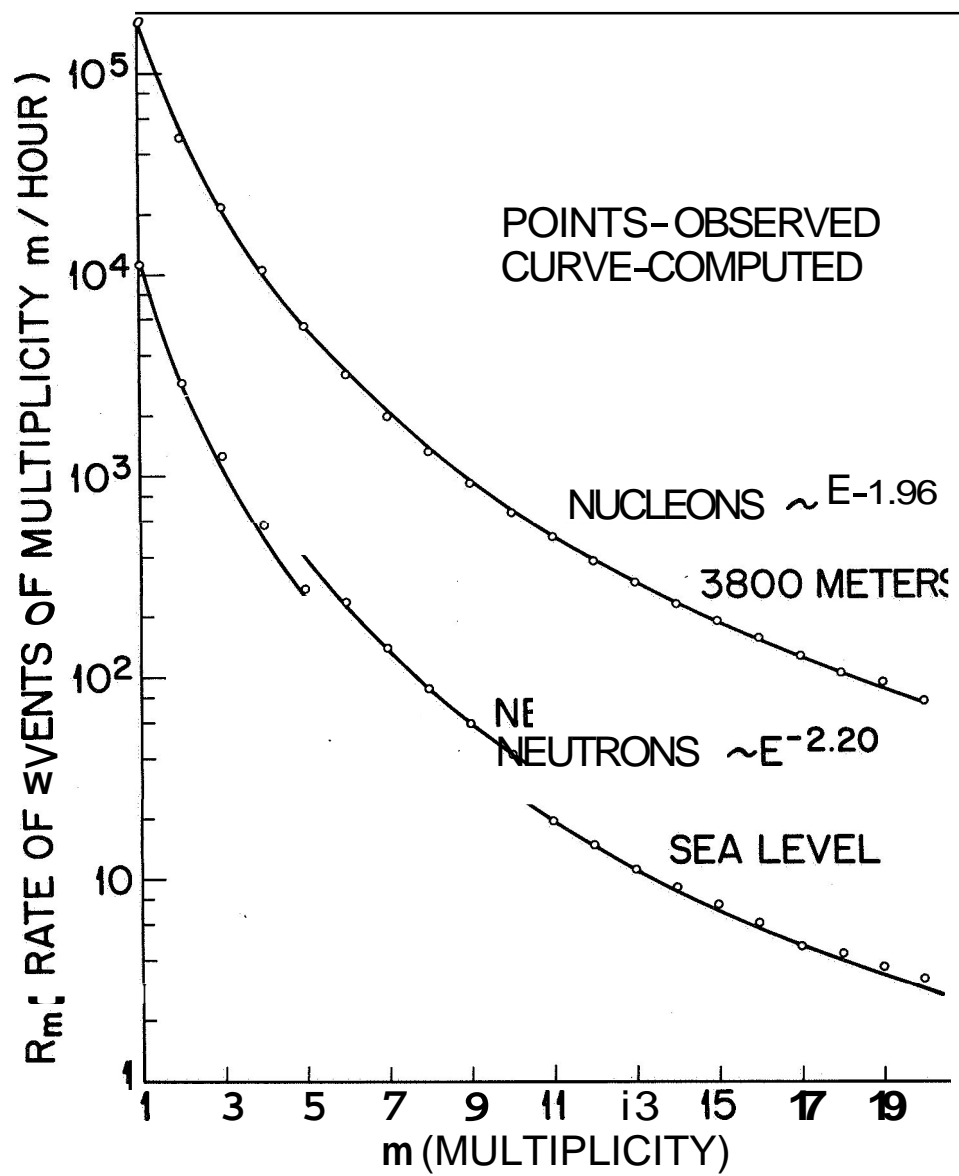
The solid curves of Fig. 3 show computed multiplicity distributions obtained by inserting the following power spectrum nucleon distributions into Equation (1) for $N(E)$:

$$N(E) = (5 \times 10^{-8}) \; E^{-2.2} \; cm^{-2} \; sec^{-1} \; MeV^{-1} \quad \text{(at sea level)}$$

and

$$N(E) = (1.5 \times 10^{-6}) \; E^{-1.96} \; cm^{-1} \; sec^{-1} \; MeV^{-1} \quad \text{(at 3800 meters)}.$$

The computed curves were normalized to the experimental data at the low multiplicity end of the spectrum and the index of the spectrum was adjusted to give the best fit of the data up to channel m = 20.

Table 1 gives typical average hourly observed rates for sea level and mountain data, together with estimated μ -meson capture, background, dead-time, and overlap corrections. Also shown is the net per-channel counting rate ratios of the two sets of data. This ratio represents prima facie evidence of an energy spectra variation with altitude. Families of curves showing the integral contribution to the rate of each multiplicity channel by nucleons of energy E and greater are given in Figs. 4 and 5. They were obtained by varying the lower limit of integration in Equation (1) and refer to the particular $N(E)$ distributions given above.

Fig. 6 shows a typical R_m distribution for all multiplicities up to m = 399; the points are based on a smoothed average of 600 hours of uncorrected mountain data. For multiplicities m ≥ 10 the data points are quite well fitted by a power law distribution where $R_m \sim m^{-3.3}$ as is shown by the curve in Fig. 6.

TYPICAL NEUTRON MULTIPLICITY COUNTING RATES

Counts/hr	m = 1	2	3	4	5	6	7	8	9	10	11	12	13	14	15	16	17	18	19	20
Sea Level																				3.2
Observed Rate	16,063	3,247	1,272	568	278	150	88.8	56.0	37.8	26.7	19.4	14.7	11.0	9.0	7.3	6.0	4.6	4.2	3.6	
μ^- Capture	-1,435	-219	-33																	
Background	-3,220	-150	-12																	
Overlap	—	—	—	—	—	—	—	—	—	—	—	—	—	—	—	—	—	—	—	3.2
Corrected Rate	11,408	2,875	1,227	568	278	150	88.8	56.0	37.8	26.7	19.4	14.7	11.0	9.0	7.3	6.0	4.6	4.2	3.6	3.2
3800-Meter Elevation																				
Observed Rate	173,660	50,758	22,056	10,775	5,683	3,250	1,996	1,301	895	642	477	359	281	219	177	145	117	95	83	67
μ^- Capture	-1,435	-219	-33																	
Background	-43,590	-2,078	-195																	
Overlap	+52,600	-822	-111	-265	-163	-71	-22	+2	+13	+16	+18	+15	+14	+12	+12	+12	+10	+10	+11	+9
Corrected Rate	181,235	47,639	21,752	10,510	5,520	3,179	1,974	1,303	908	658	495	374	295	231	189	157	127	105	94	76

	m = 1	2	3	4	5	6	7	8	9	10	11	12	13	14	15	16	17	18	19	20
Sea Level	15.9	16.6	17.7	18.5	19.8	21.2	22.2	23.3	24.0	24.6	25.5	25.4	26.8	25.6	25.9	26.2	27.6	25.0	26.1	23.8

Fig. 4   A family of curves showing the integral contribution at sea

level to the rate of each multiplicity channel by nucleons
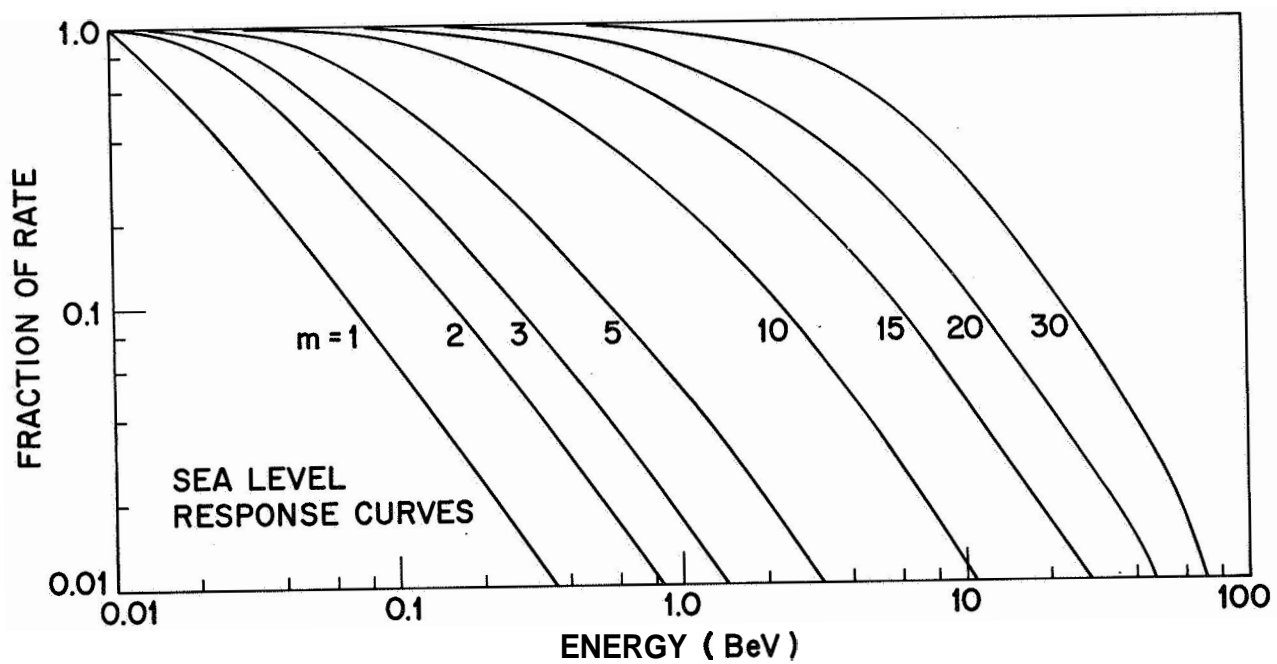
of energy E and greater.

SEA LEVEL RESPONSE CURVES

Fig. 5   **A** family of curves showing the integral contribution at 3800

meter elevation to **the** rate of each multiplicity channel by
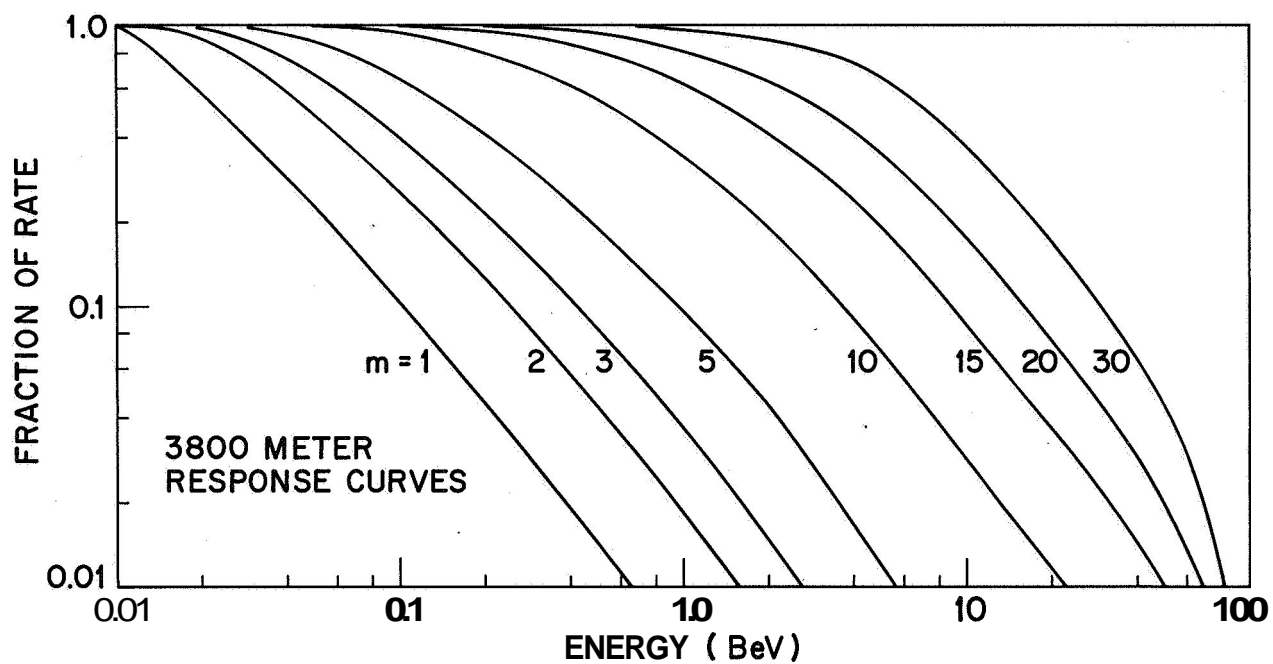
nucleons of energy E and greater.
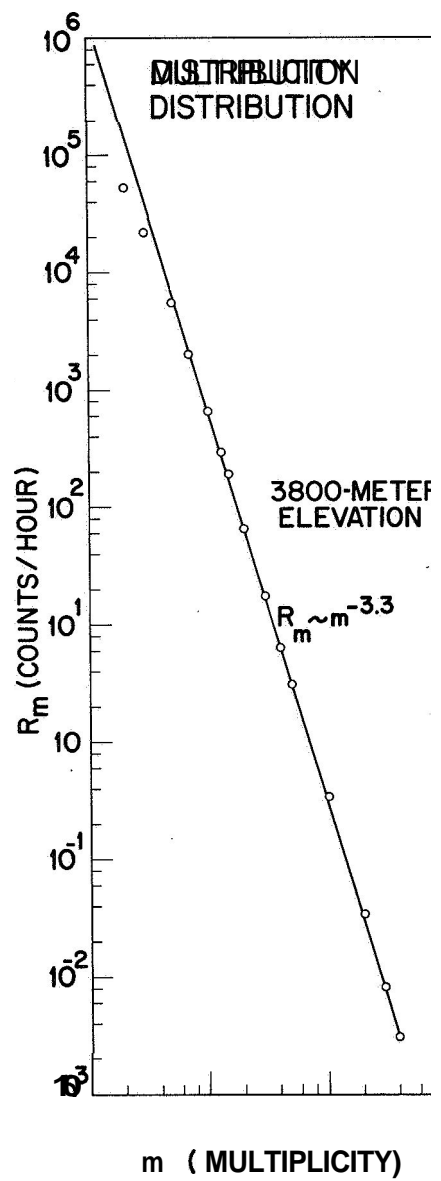
3800 METER RESPONSE CURVES

Fig. 6   Typical observed multiplicity distribution, R_m, for all multi-
plicities up to m = 399.   The points are based on an average
of 600 hours of uncorrected mountain data.   The curve is the
locus of points described by the relationship $R_m \sim m^{-3.3}$

MULTIPLICITY DISTRIBUTION

3800-METER ELEVATION

$R_m \sim m^{-3.3}$

R_m (COUNTS / HOUR)

m   (MULTIPLICITY)

IV PRESSURE COEFFICIENTS

The counting rate of a neutron monitor exhibits an exponential dependence on the air mass above the detector as given by

$$I = \bar{I} \exp \beta (p-\bar{p}) \tag{3}$$

where I is the observed intensity at pressure p, $\bar{I}$ is the intensity at some standard pressure $\bar{p}$ and β is the pressure coefficient. Pressure coefficients as a function of multiplicity were determined by performing a regression analysis of ln I on p for each multiplicity channel, the best results being obtained from intervals of a few days duration which were selected to encompass large pressure variations but no pronounced primary intensity fluctuations. Coefficients are given for multiplicity channel rates m = 1 through 9 for sea level data and m = 1 through 15 for mountain data. Table II lists the observed coefficients and Fig. 7 gives a plot of coefficients versus multiplicity. The relatively smaller observed values shown for the low multiplicity sea level coefficients can be explained as follows: muons have a longer absorption length than nucleons, hence they appear in increasing fractional abundance with increasing atmospheric depth. This fact and the lower mean multiplicity associated with μ-capture neutron production (Hughes 1961) have the effect of reducing the low multiplicity pressure coefficients with respect to those for higher multiplicities whose rates receive no contributions from such events. On the basis of this explanation, the observed coefficients are consistent with a 9, 6. 5 and 2. 5 percent μ-capture contribution to the counting rates of the sea level m = 1, 2 and 3 channels respectively. The mountain elevation counting ratee receive no significant contribution from this source. Pressure coefficients have also been determined by the Lapointe and Rose (1962) method of successive

TYPICAL BAROMETRIC PRESSURE COEFFICIENTS

Multiplicity Channel	Sea Level			3800–Meter Elevation		
	$(\times 10^{-2})$	β	mm Hg^{-1}	$(\times 10^{-2})$	p	mm Hg^{-1}
m = 1	0.790	± 0.04		0.960	a 0.010	
2	0.910	± 0.047		0.950	± 0.011	
3	1.00	± 0.068		1.020	± 0.015	
4	1.060	± 0.11		1.030	± 0.018	
5	0.980	± 0.15		0.990	± 0.021	
6	0.930	± 0.20		1.090	± 0.028	
7	0.700	± 0.28		1.130	± 0.042	
8	1.10	± 0.37		1.070	± 0.050	
9	1.45	f0.41		1.190	± 0.059	
10				1.120	± 0.078	
11				1.190	± 0.086	
12				1.090	± 0.104	
13				1.150	± 0.112	
14				1.290	± 0.129	
15				1.000	± 0.137	

Fig. 7   Pressure coefficient β as a function of multiplicity for **sea**

level and 3800 meter elevation.
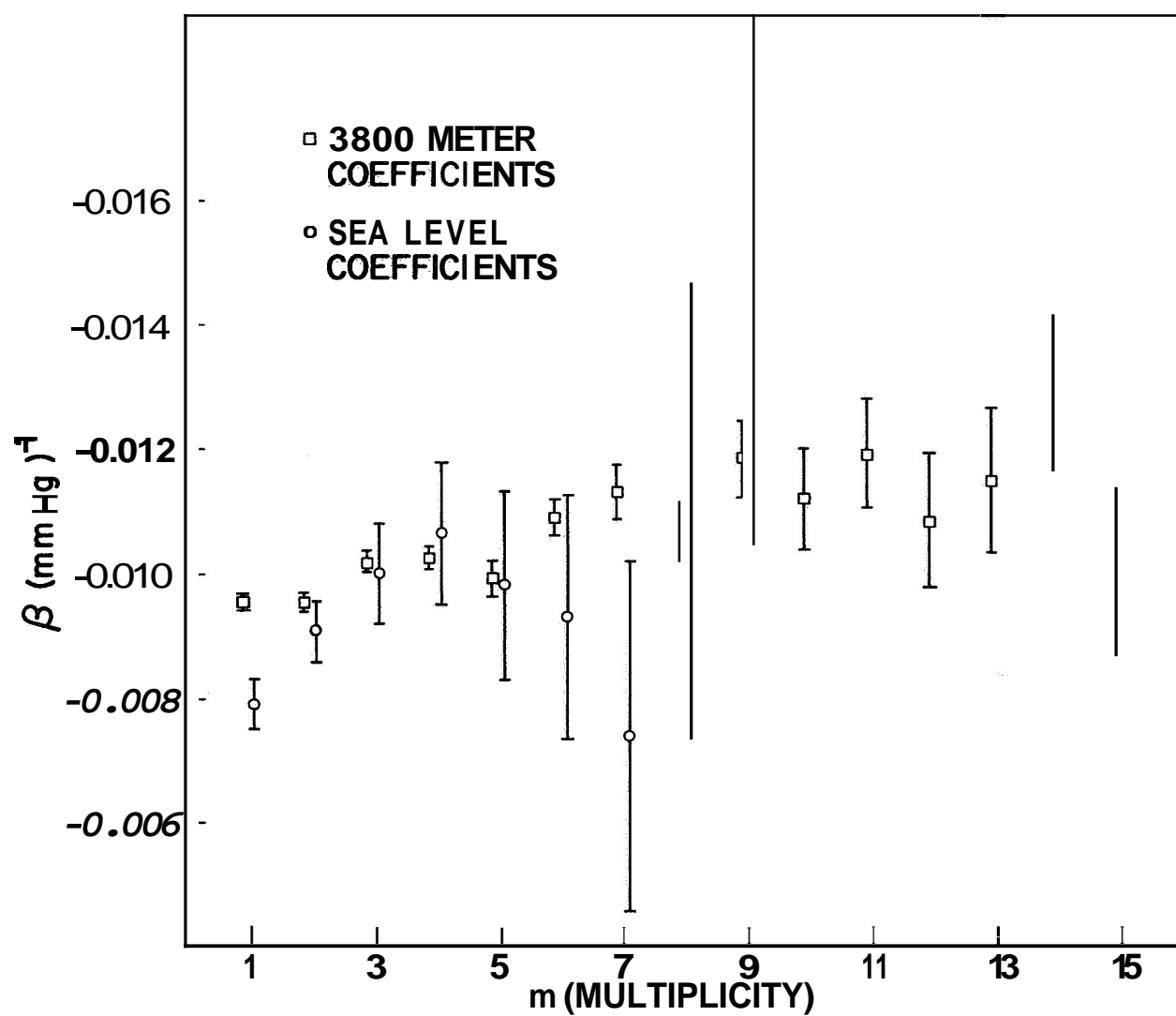
differencing.   This method minimizes the effects of small gradual changes in primary intensity.   It is developed as follows: if Equation **(3)** is written for *two* successive days, i.e.,

$$I_1 = \bar{I}_1 \exp \beta \ (p_1 - \bar{p}) \text{ and } I_2 = \bar{I}_2 \exp \beta \ (p_2 - \bar{p}),$$
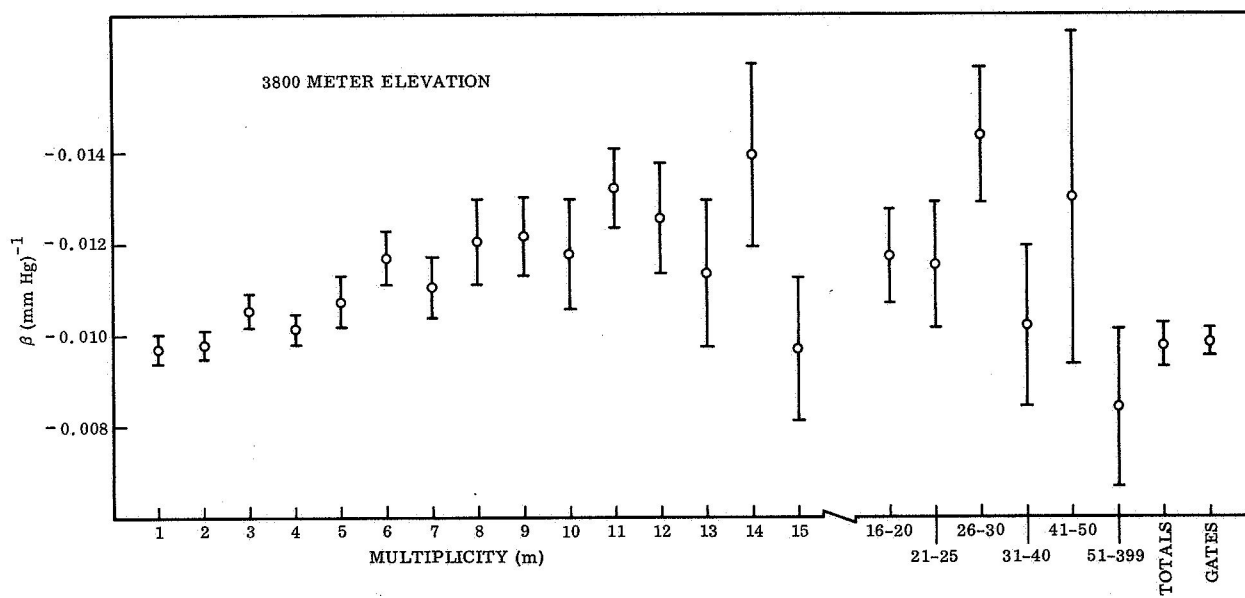
then

$$\frac{I_1}{I_2} = \ln \ \frac{\bar{I}_1}{\bar{I}_2} + \beta \ (p_1 - p_2) \ .$$

If the primary intensity has not changed appreciably between the two days, then $\bar{I}_1 \simeq \bar{I}_2$ and $\ln \frac{\bar{I}_1}{\bar{I}_2} \approx O$. Hence a regression analysis is performed of $\ln \frac{I_1}{I_2}$ on $(p_1 - p_2)$ to determine β . In order to eliminate the possible effects of diurnal variations, daily means were used in the regression analysis. It was required that a daily mean be based on at least 18 hours of data in order to be included in the analysis.   Work on the determination of barometric co-efficients for ordinary neutron monitors using the method of successive differ-encing have recently been reported by Bachelet et al. (1965) and Griffiths et al. (1966).   The results of the present work using this method to give individual multiplicity channel coefficients for 3800 meter elevation data are shown in Fig. 8.   Coefficients for the total neutron rate and the gate rate, shown on the extreme right of the plot, have nearly the same value as those for the low multiplicity channels, which is to be expected from the fact that these channels dominate both the total and gate rates.

V   DAILY **MEAN** INTENSITY

The most statistically significant monitor data with respect to the total incident nucleon intensity is the gate counting rate.   This is because there is

Fig. 8   Pressure coefficient β versus multiplicity for 3800 meter elevation as determined by the method of successive differencing. Channels m = 16 and above have been grouped in order to improve the accuracy of the results. The last two points on the right give the coefficients for the total neutron count and the gate count.

only one gate per event, independent of the multiplicity, hence the variance of this quantity is smaller than that of the numerically greater total neutron count which is effected by multiplicity (see Appendix C). Fig. 9 shows the daily mean hourly gate counting rate for all 3800 meter elevation data through June 30, 1966. The plotted rates have been corrected for deadtime and reduced to a standard pressure of 645 millibars. Fig. 9 also shows daily sums of the 3-hour geomagnetic disturbance indices K_P (from compilations of Solar-Geophysical Data, U. S. Department of Commerce).

Gaps in the data represent intervals in which the information was lost due to power failure, instrumental malfunction, or in the case of days 92-118, to an improbable accident which caused the loss of bzrometric readings for that interval.

VI FORBUSH DECREASE OF MARCH 23, 1966

The year of contract supported operations (June 22, 1965 to June 22, 1966) encompassed the period of minimum solar activity and was in general a quiet time as far as cosmic ray activity was concerned. The most interesting single event was a Forbush decrease which began at about 0400 March 23, 1966, local time. Fig. 10 shows the hourly gate rate for a number of days before and during the decrease. The plotted data is pressure corrected but not deadtime corrected. Since the energy response is known as a function of multiplicity, the event was studied by taking the ratios of corresponding channel mean counting rates for a 140-hour period during the decrease to a 158-hour period before the decrease. The higher multiplicity channels were grouped in order to improve the statistical accuracy of the results. The ratios, shown in Fig. 11, indicate a modulation of about 5 percent in the low multiplicity channels,

Fig. 9   Daily mean hourly gate counting rate for all White Mountain

(3800 meter) data through June 30, 1966. The rates have

been corrected for deadtime and reduced to a standard pres-

sure of 645 millibars.   Also shown are daily sums of the 3-

hour geomagnetic disturbance indices K_P (from compilations

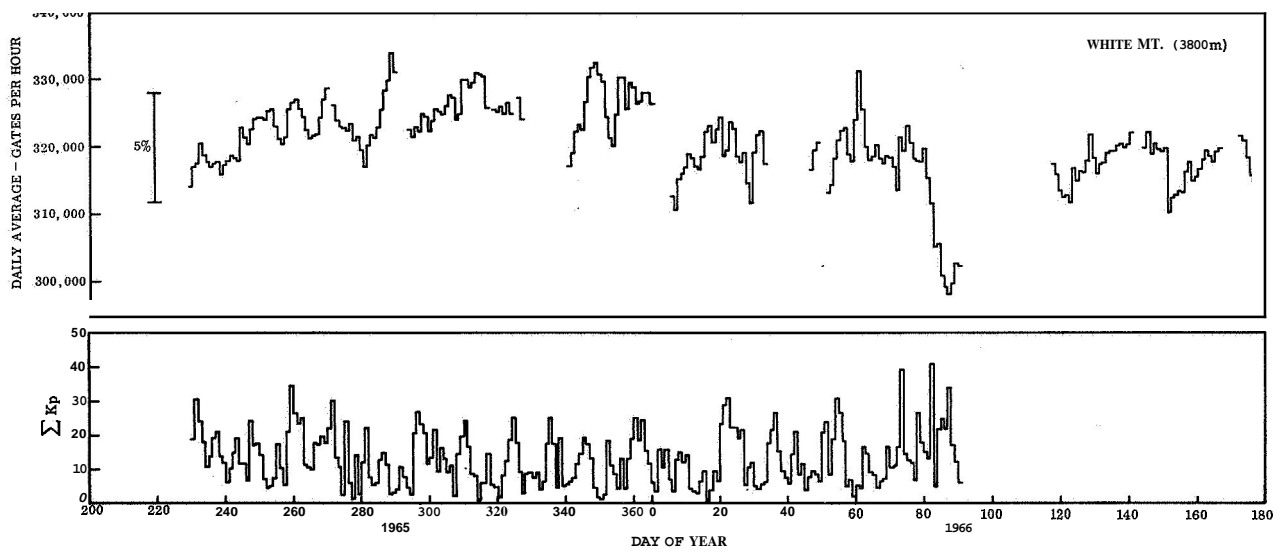of Solar-Geophysical Data, U. S. Department of Commerce).

WHITE MT. (3800m)

DAILY AVERAGE – GATES PER HOUR

340,000
330,000
320,000
310,000
300,000

5%

$\sum Kp$

50
40
30
20
10
0

200 220 240 260 280 300 320 340 360 0   20   40   60   80   100 120 140 160 180

1965   1966

DAY OF YEAR

Fig. 10   The hourly gate rate spanning a period of time about the beginning of the Forbush decrease of March 23, 1966.
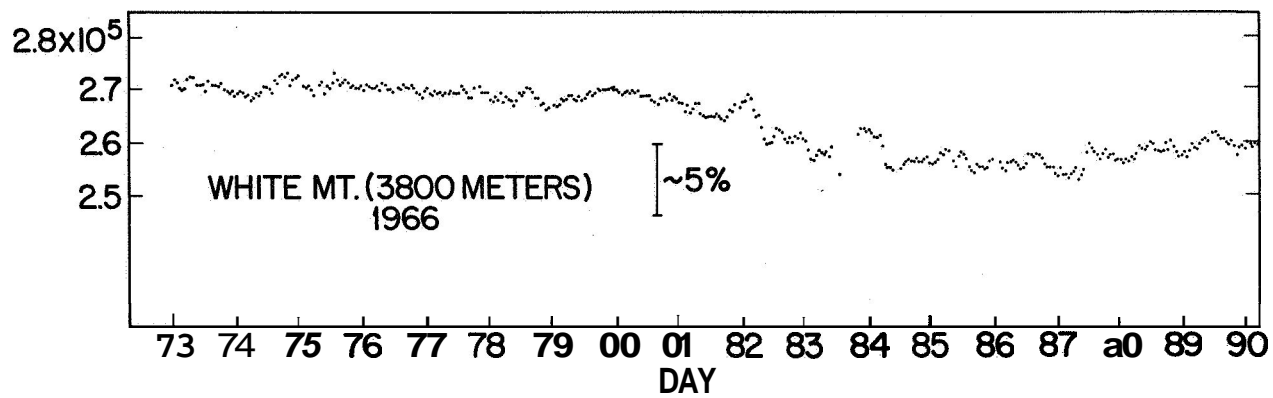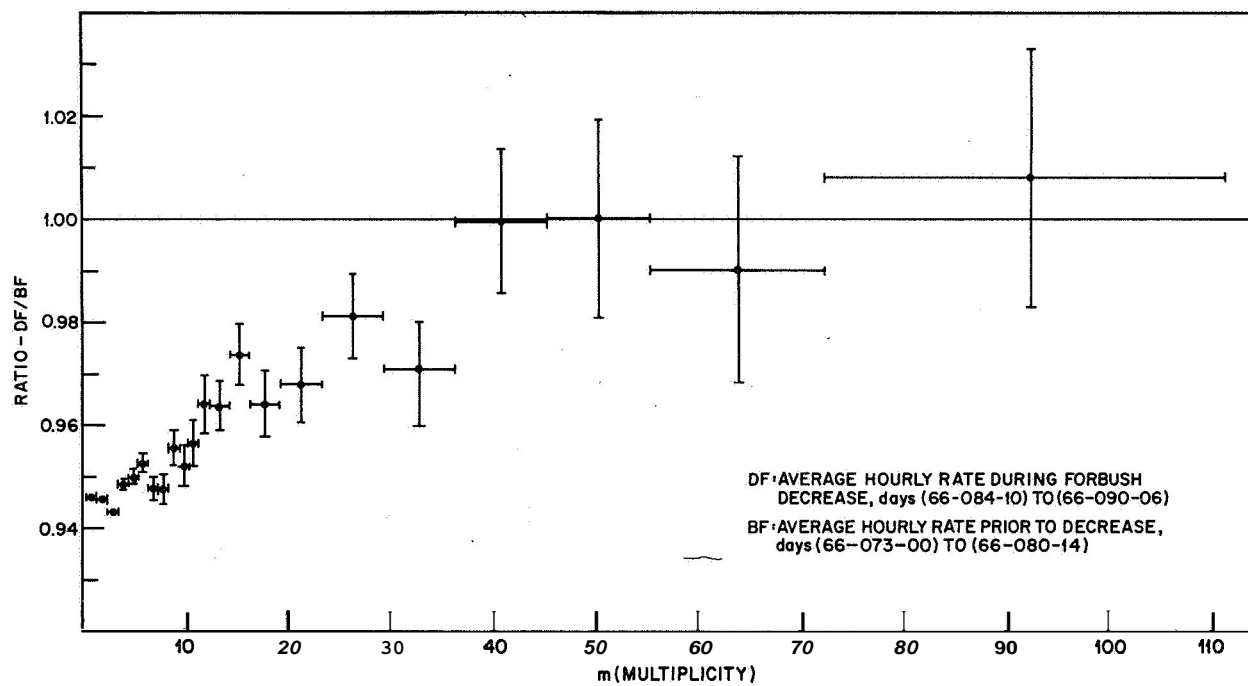
WHITE MT. (3800 METERS)
1966

~5%

73 74 75 76 77 78 79 00 01 82 83 84 85 86 87 a0 89 90
DAY

Fig. 11   Ratio of the average hourly gate rate for a period of time during

the Forbush decrease of March **23,** 1966 to a similar length

period before the decrease.

RATIO – DF/BF

m (MULTIPLICITY)

DF:AVERAGE HOURLY RATE DURING FORBUSH
DECREASE, days (66-084-10) TO (66-090-06)

BF:AVERAGE HOURLY RATE PRIOR TO DECREASE,
days (66-073-00) TO (66-080-14)

diminishing toward higher multiplicities and finally disappearing at about

channel **40.** The median response energy of the highest effected channels

is on the order of 6 BeV, corresponding to a primary energy of roughly

30 BeV, which is well above the equatorial vertical cut-off energy of ~

15 BeV.

VII DIURNAL INTENSITY VARIATION

An investigation of the multiplicity dependence of diurnal intensity

variations was carried out for a number of selected intervals by the use of

auto-covariance and power spectrum analysis techniques (Blackman and

Tukey, 1959). Of the intervals investigated one suggested by Lindgren (1966)

showed the greatest variation. The data record studied began at midnight

April 29, 1966 UT (66-119-00) and was of about 12 days duration including

two interruptions caused by power line failures. However, the auto-covariance

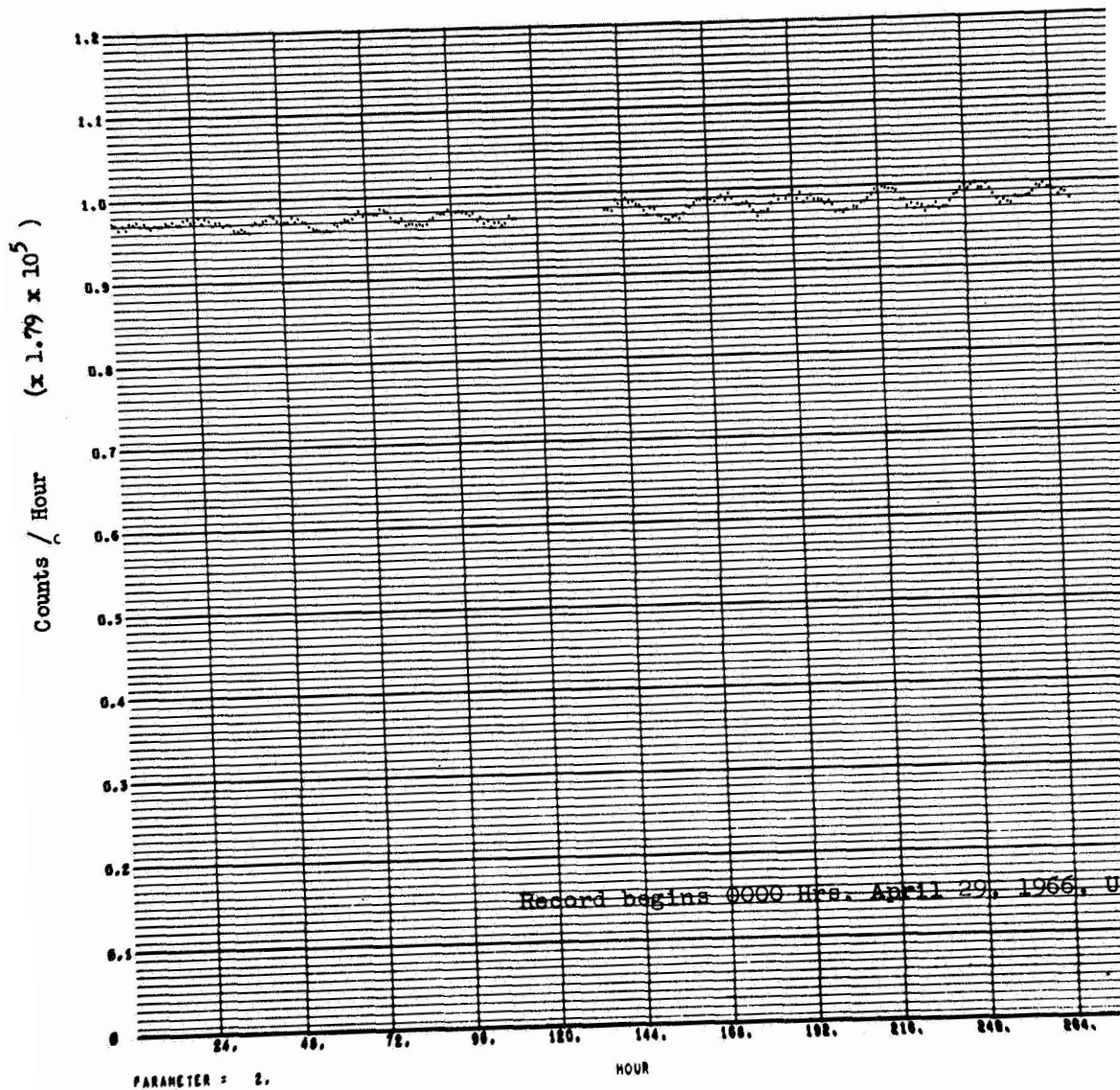program is written so as to be able to handle such record gaps without diffi-

culty.

Figs. 12 through 17 show the normalized gate and multiplicity channel

rates for m = 1 through 5 respectively for the period in question, the normali-

zation factor being indicated on each plot. Figs. 18 through 23 show the power

spectra of the auto-covariance function for the respective channels. The peak

at 2KF = 10 corresponds to the diurnal frequency. The power is plotted at

integral values of the function 2KF, where K = 125 is the maximum lag and F

is the hourly frequency. The maximum amplitude of the intensity variation in

the gate channel was estimated to be on the order of 1.5 percent on day 66-128

and the results derived from the auto-covariance study over the entire interval

Figs. 12 through 17   The gate counting rate and multiplicity channel rates for m = 1 through 5 during a period of enhanced diurnal intensity variation.   The data are reduced to a standard pressure of 645 millibars and are corrected for overlap and instrumental deadtime.
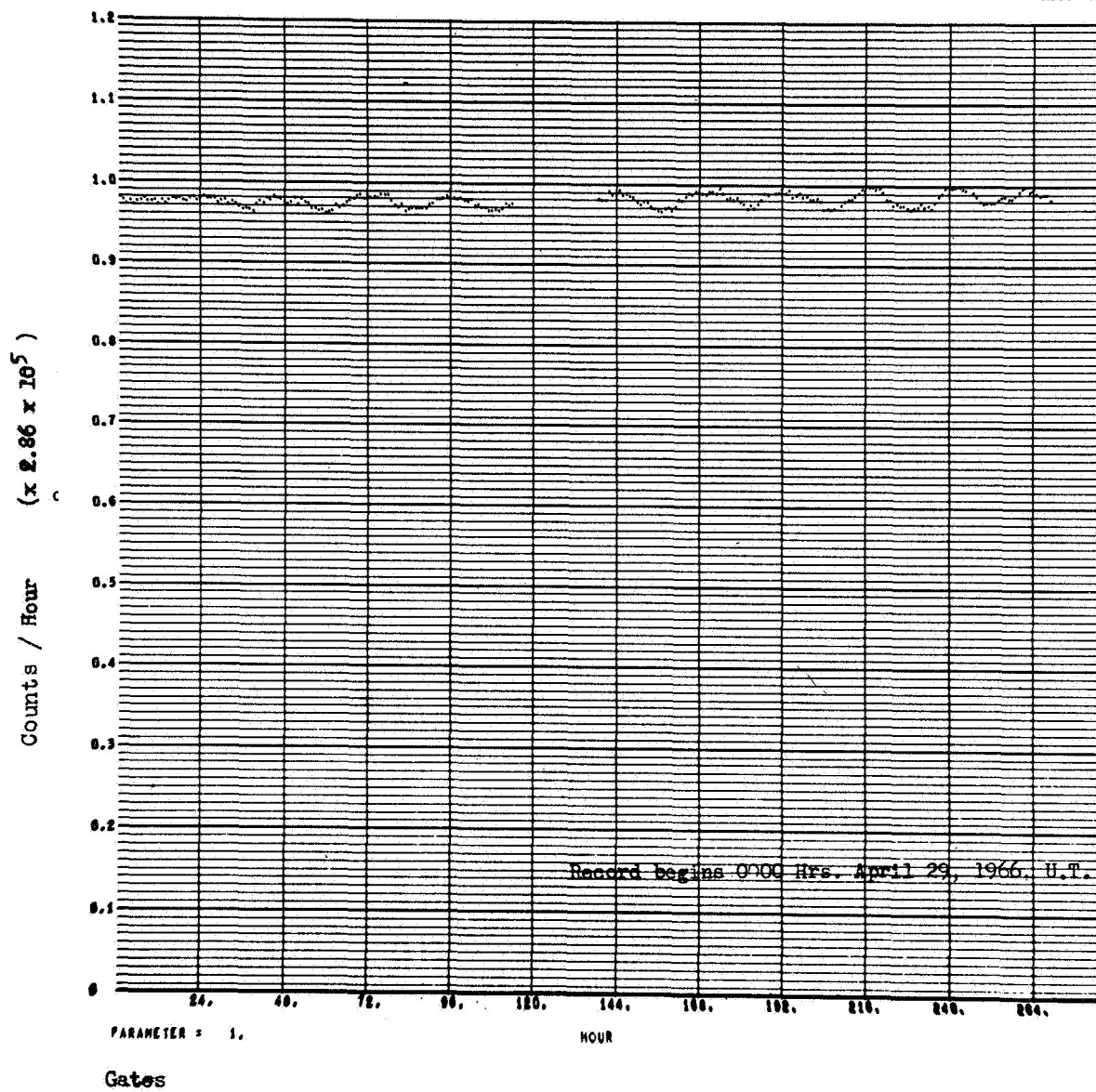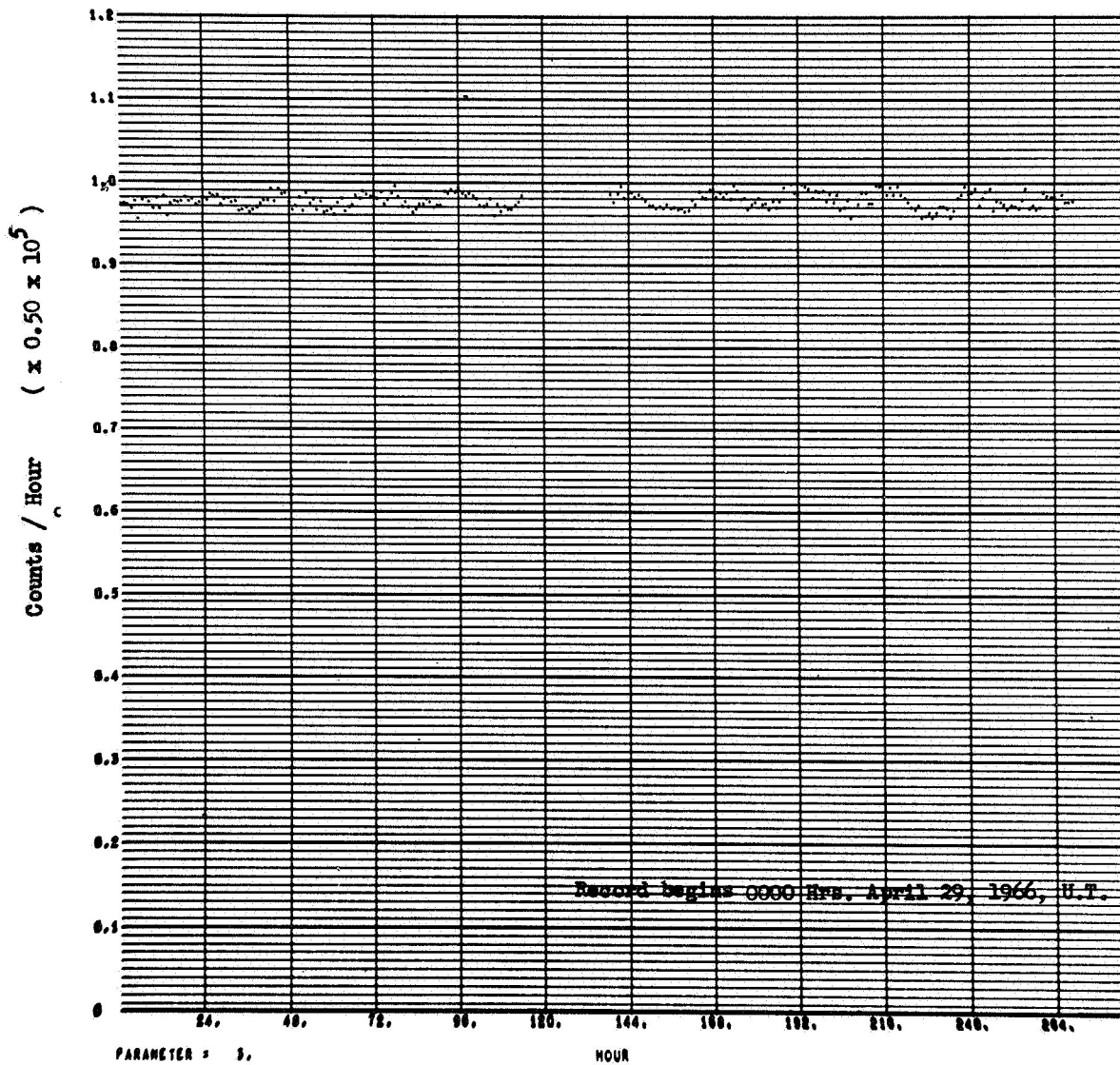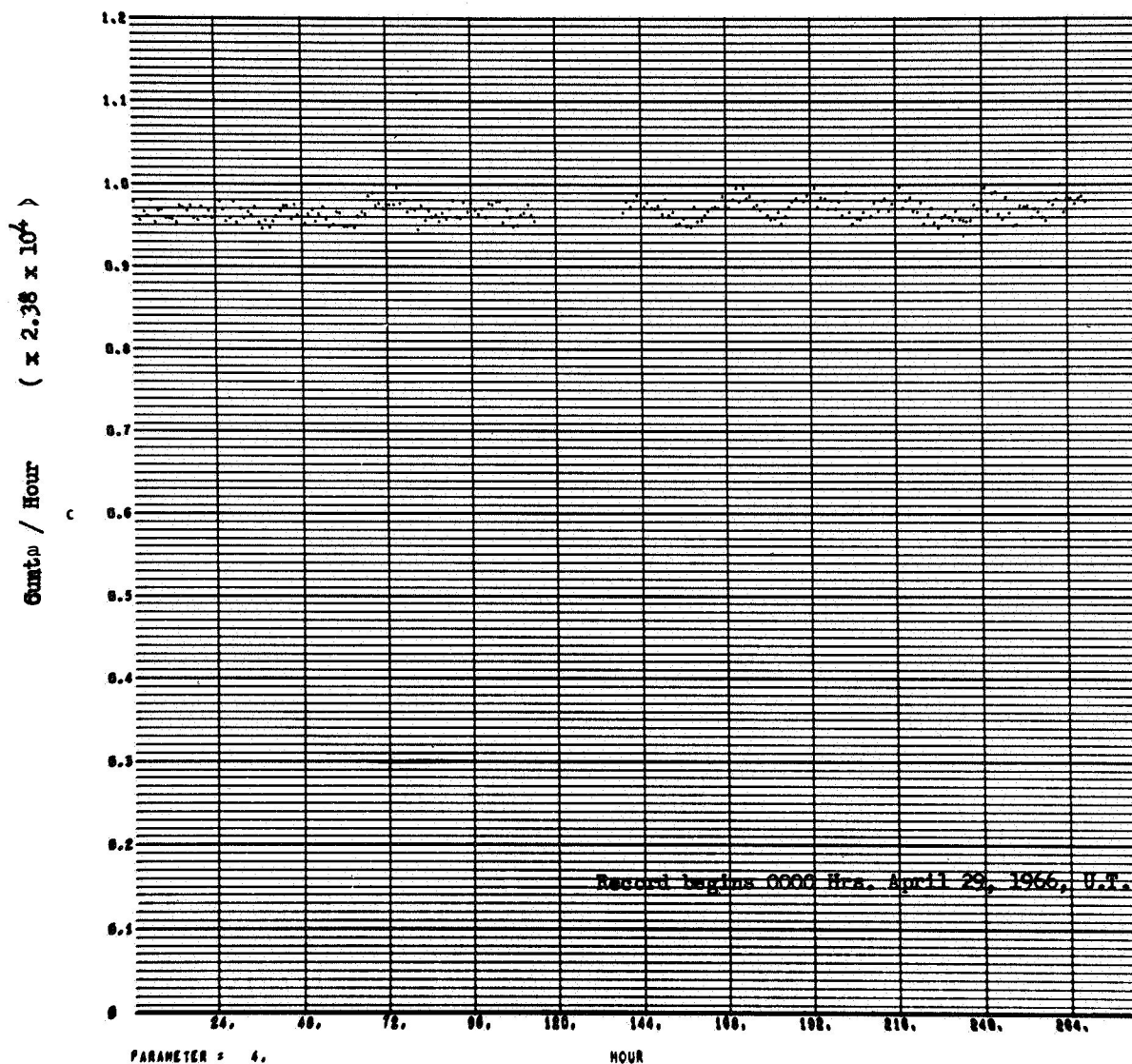
Counts / Hour   (x 2.86 x 10^5)

Record begins 0000 Hrs. April 29, 1966, U.T.

PARAMETER = 1.

HOUR

Gates

Figurer 12

Record begins 0000 Hrs. April 29, 1966, U

PARAMETER = 2.

HOUR

Counts / Hour   (x 1.79 x 10^5)

Figure 14

PARAMETER : 3,

m = 2

Record begins 0000 Hrs. April 29, 1966, U.T.

Counts / Hour (x 0.50 x 10^5)

HOUR

Record begins 0000 Hrs. April 29, 1966, U.T.

PARAMETER = 4.   HOUR

m = 3   Figure 15

Counts / Hour   (x 1.08 x 10^4)

Record begins 0000 Hrs. April 29, 1966, U.T.

PARAMETER : 5,   HOUR

m = 4   Figure 16

Counts / Hour   (× 5.58 × 10³)

Record begins 0000 Hrs. April 29, 1966, U.T.

PARAMETER =   6,   HOUR
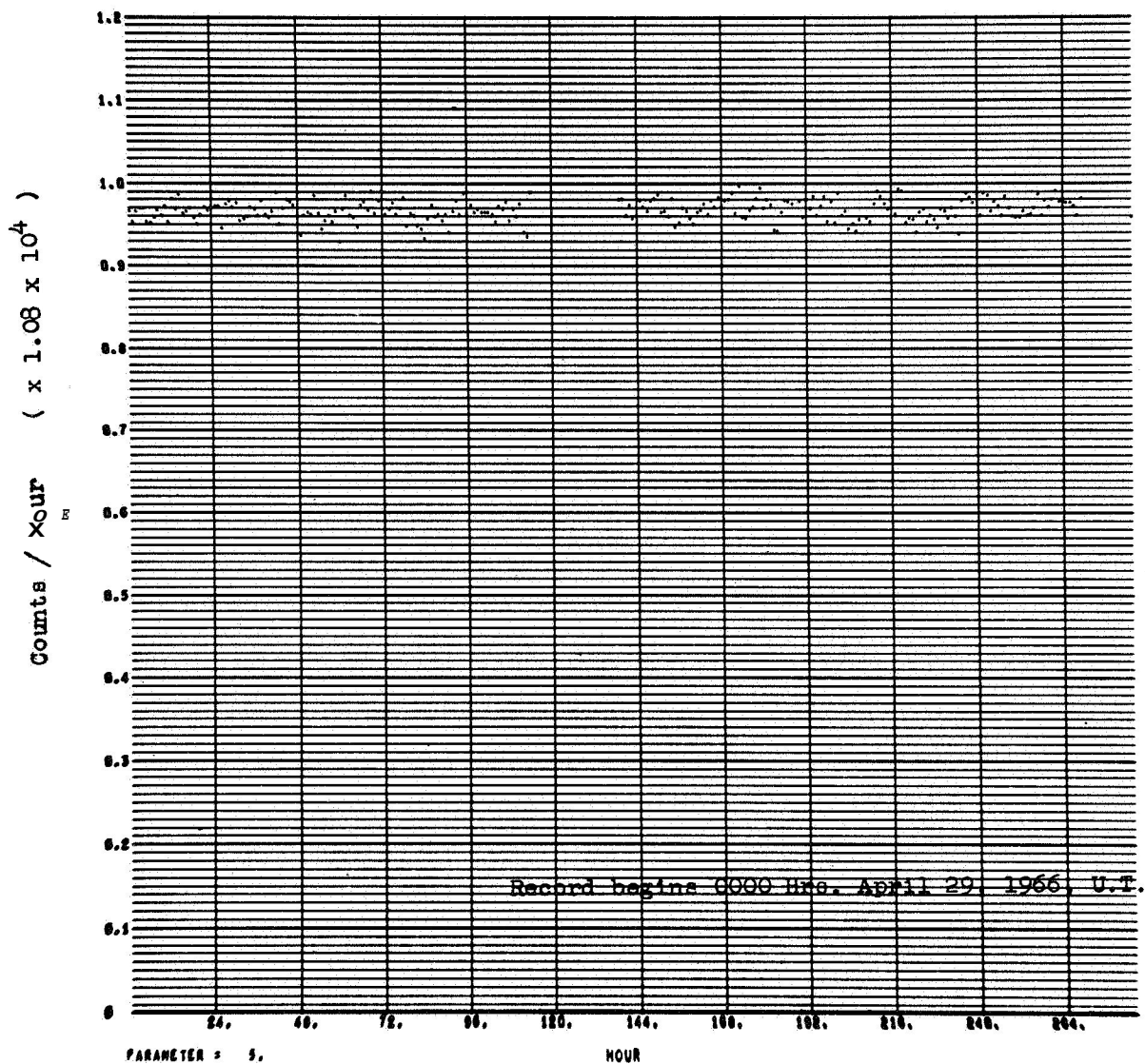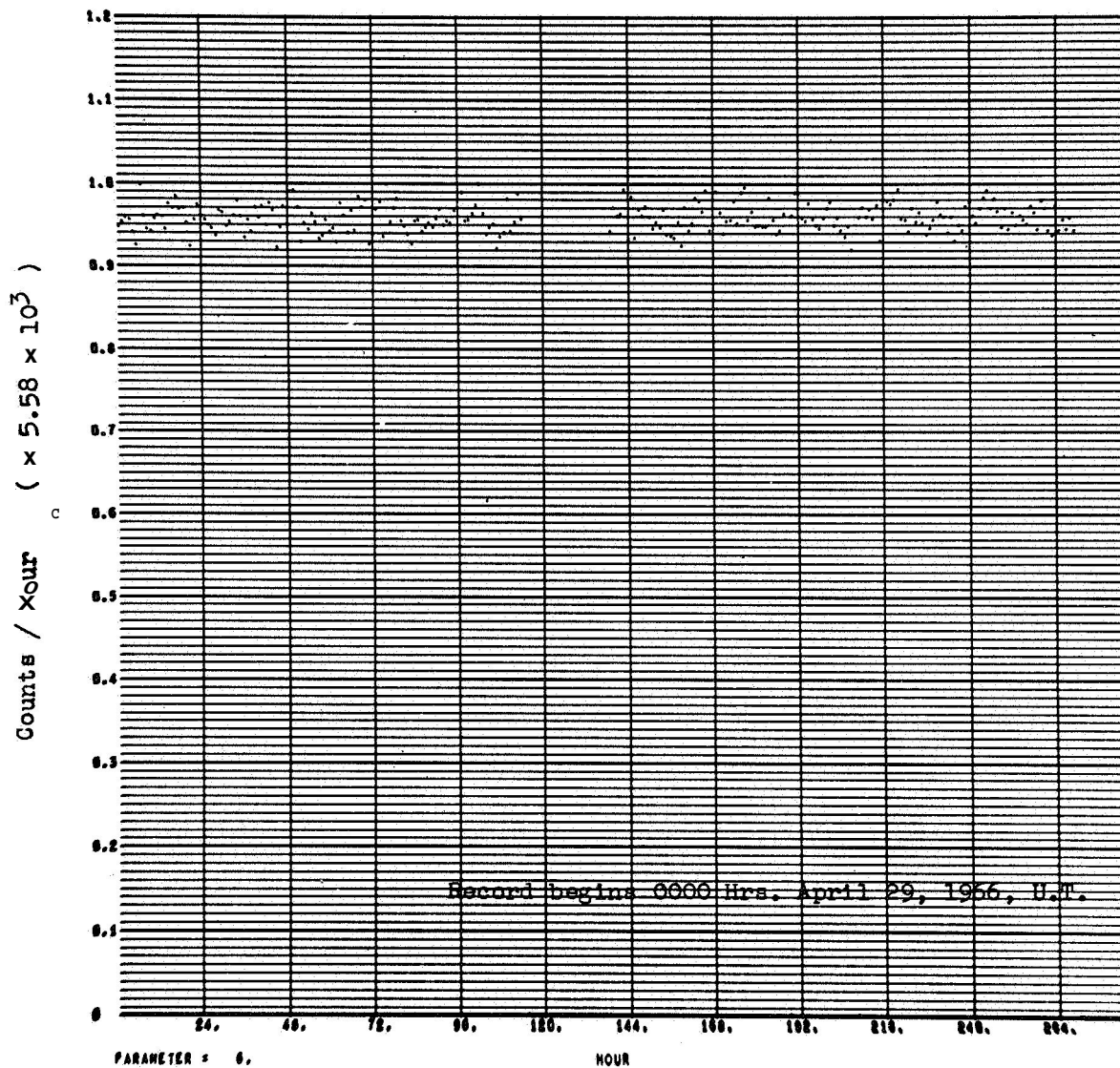
m = 5

Figure 17

Figs. 18 through 23   Relative power density of the auto-covariance
function for the preceding counting rate data.
The peak at $2KF = 10$ corresponds to the di-
urnal frequency.   The power is plotted at inte-
gral values of the function $2KF$, where $K = 125$
is the maximum lag in hours and F is the hourly
frequency.

Figure 18

Figure 19
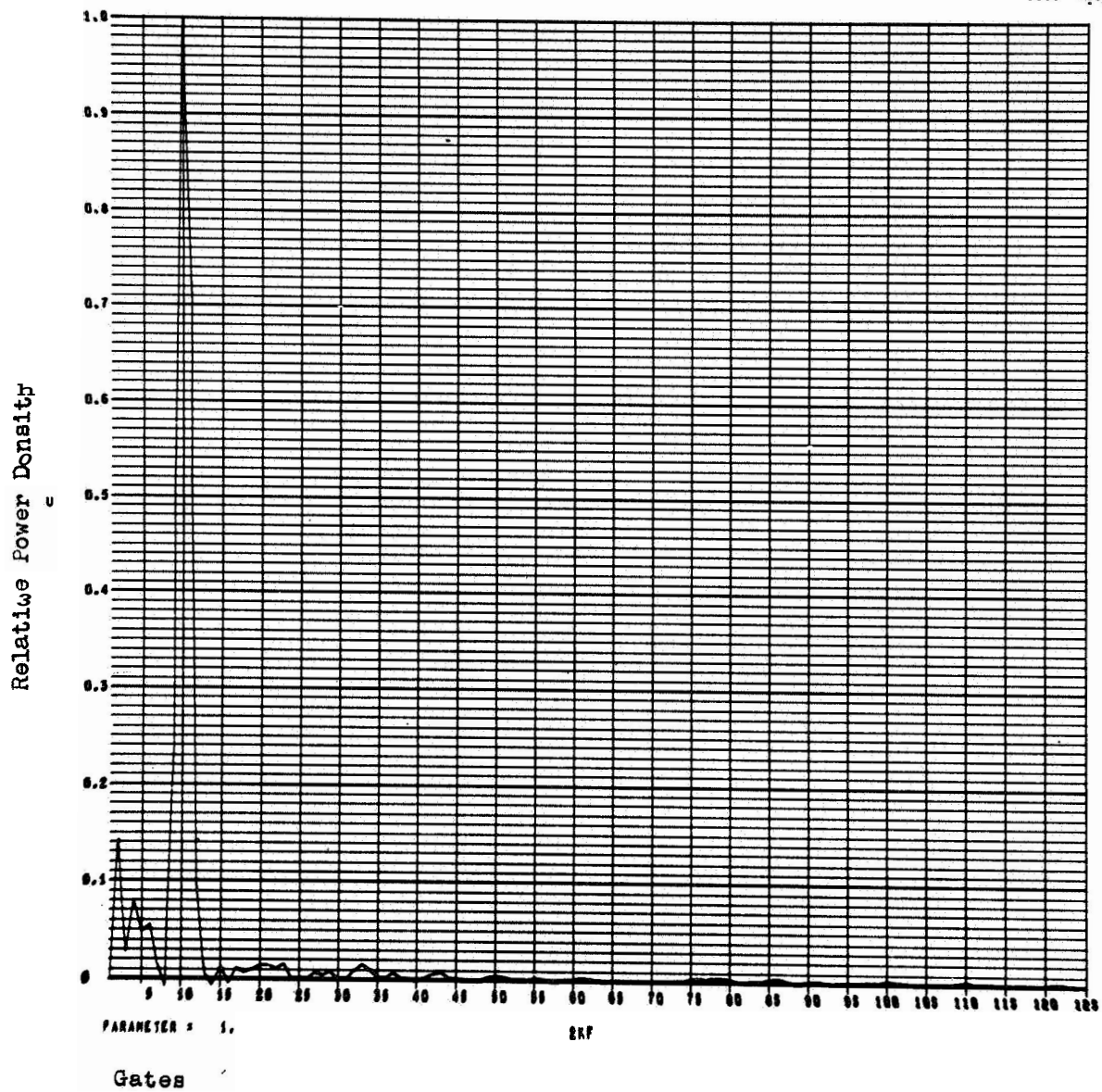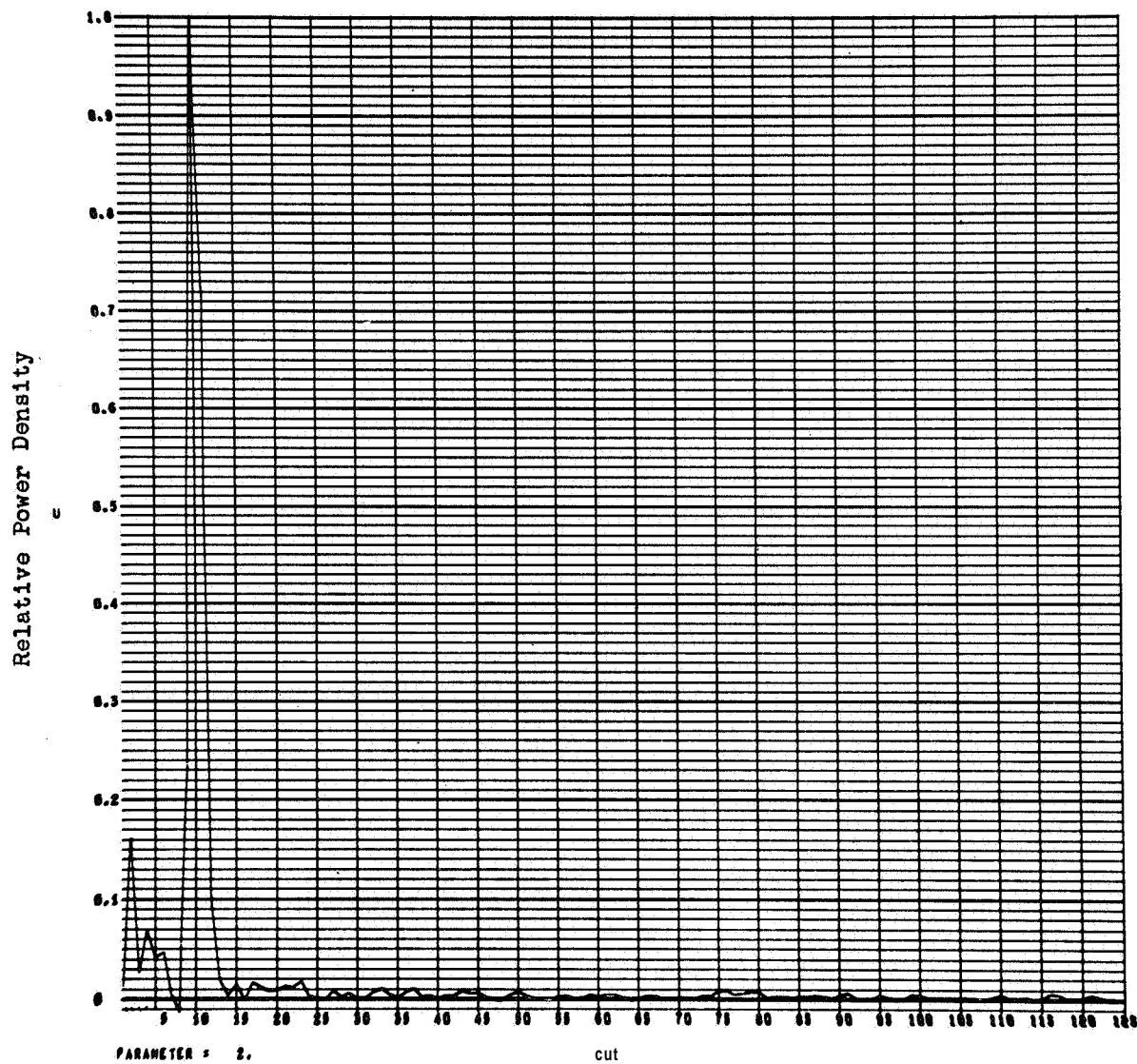
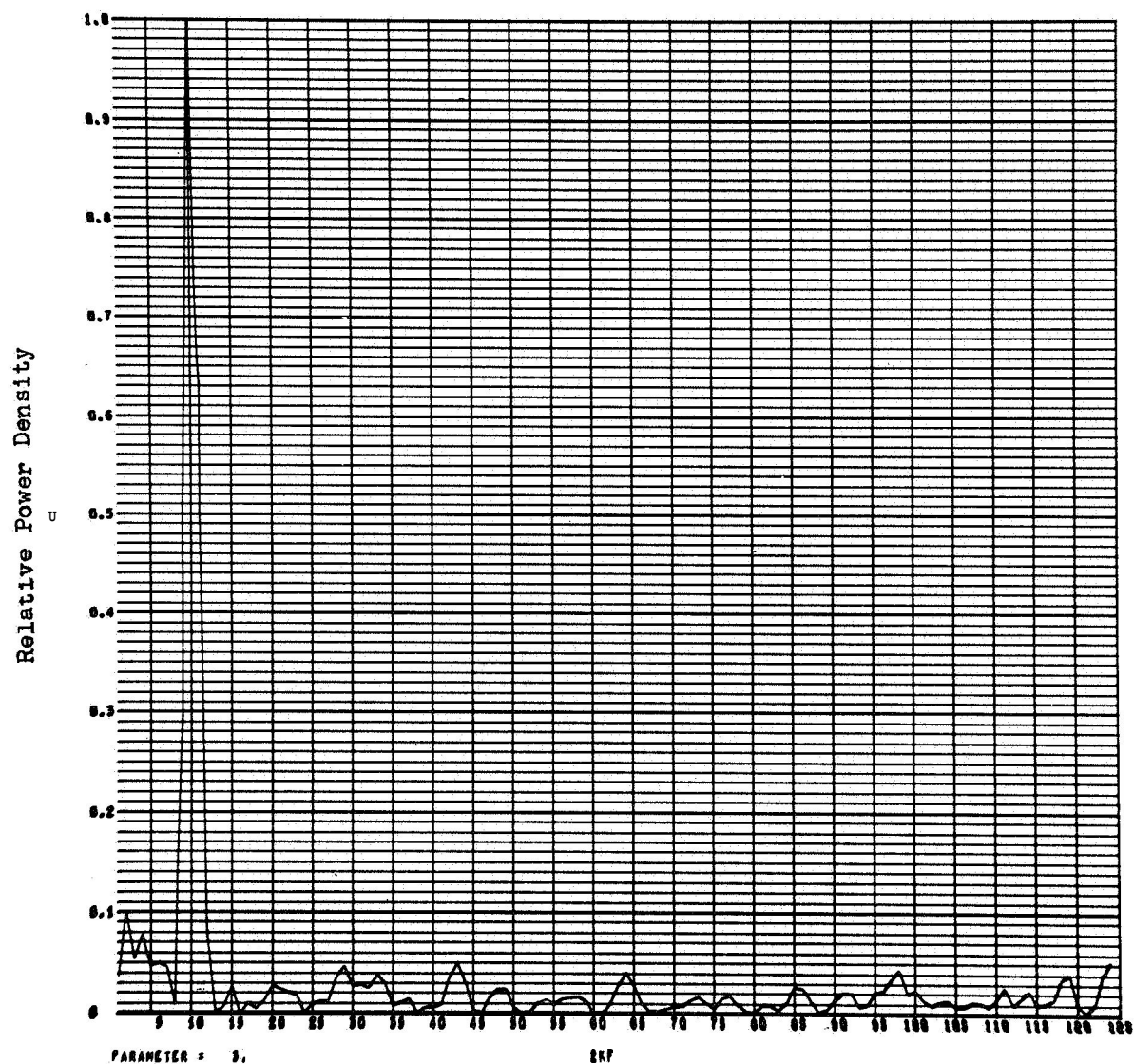PARAMETER = 3.

2KF

m = 2

Figure 20

Figure 21

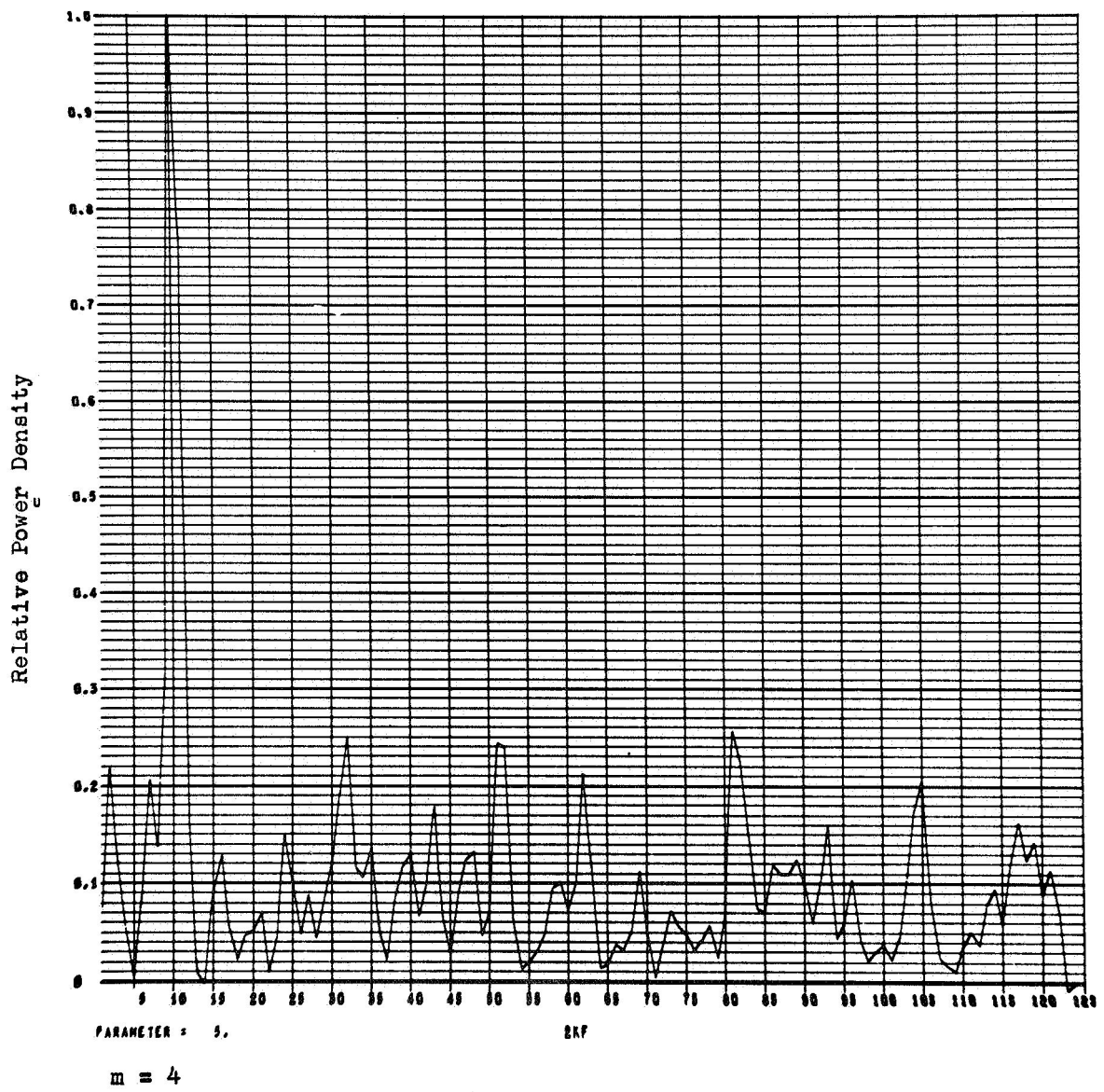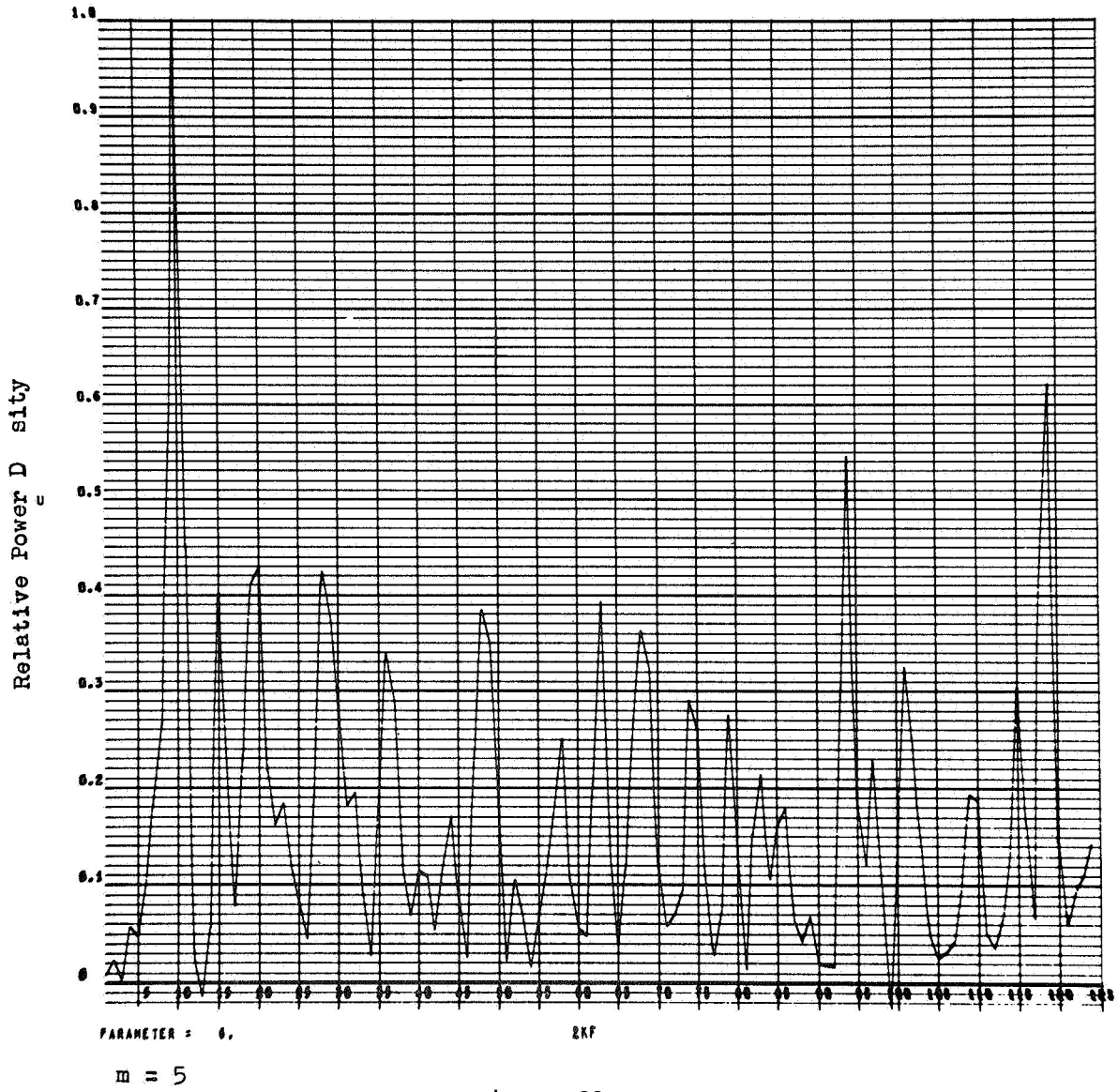PARAMETER :   5.   2KF

m = 4
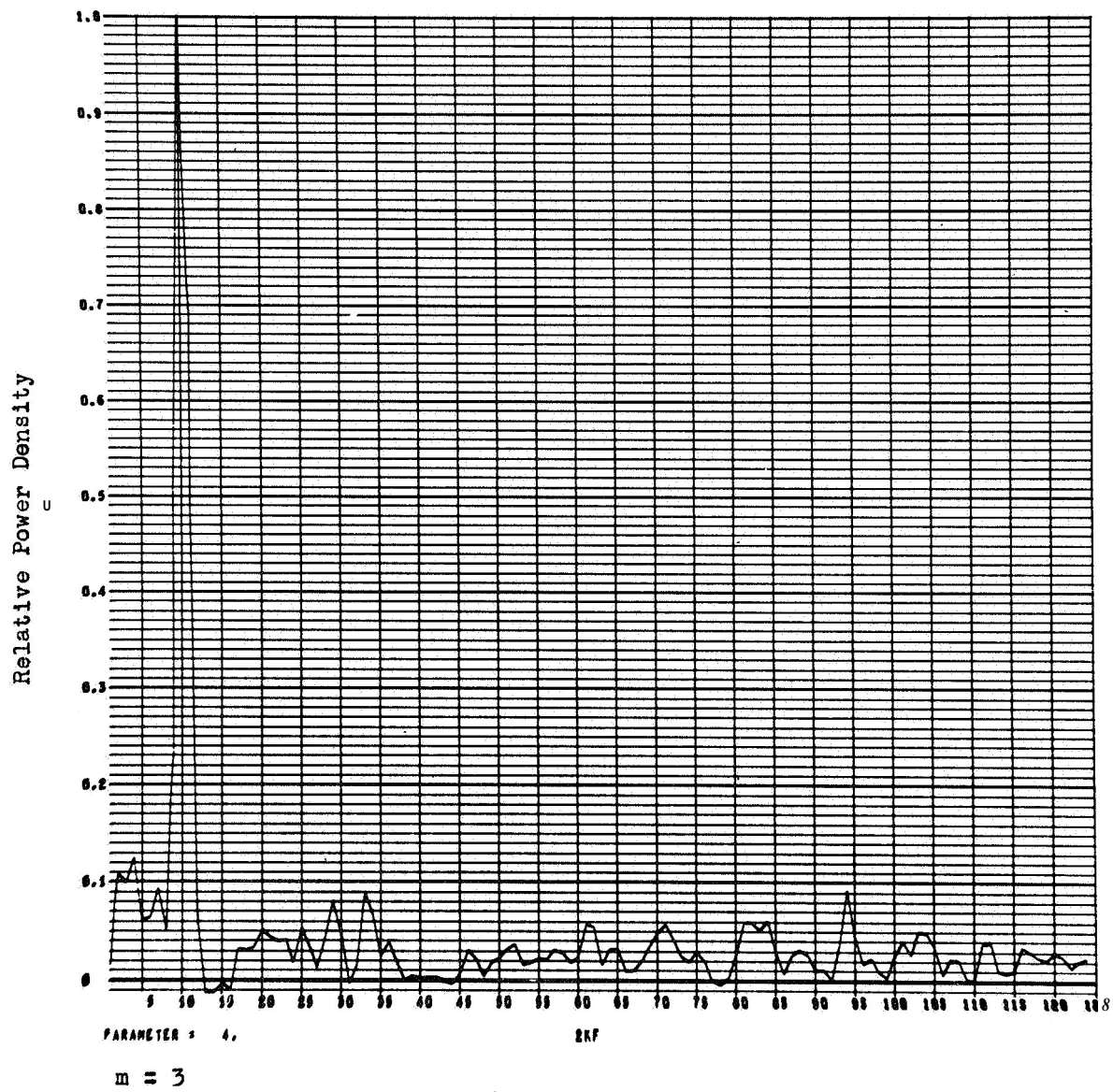
Figure 22

Figure 23

gave an amplitude of 0.65 percent for the gates and amplitudes of 0.67, 0.65, 0. **70,** 0.56 and 0. 55 percent for channels m = 1 through 5 respectively, with an estimated accuracy of about **30** percent. Studies are continuing to determine the highest channel at which the diurnal effect can be discerned. The maximum of the diurnal variation occurred at about midnight UT and there was no obvious phase shift between the various multiplicity channels.

VIII SEA LEVEL LATITUDE SURVEY EVALUATION STUDY

A study was made of the desirability of and problems involved in conducting a geomagnetic latitude survey with the multiplicity monitor similar to those car-ried out with ordinary neutron monitors by Pomerantz (1958), Sandstrom (1962) and others. It has been concluded that it is highly desirable to conduct such an experiment for the purpose of calibrating the monitor's response against the known shape of the primary spectrum and vertical cut-off rigidity profile. The experiment will provide a direct calibration of the individual multiplicity channel response as a function of primary energy, independent of atmospheric cascade models. The latitude survey is also important with respect to the establishment of the multiplicity monitor as a significant geophysical research tool.

The actual performance of the experiment would be fairly simple, as the complete observatory enclosure can be loaded as deck cargo on board a cargo liner at San Francisco and shipped on a round trip voyage to the Southwest Pacific area. The monitor would be operated continuously during the voyage and the data analyzed with respect to the ship's geomagnetic coordinates.

IX HIGH ALTITUDE AIRCRAFT OPERATIONS

Under the high counting rate conditions which would prevail at aircraft

elevations, the LMSC monitor would not be able to function as a multiplicity monitor but only as a total intensity detector. This is because it is not possible to resolve individual multiplicity events when the average time between events approaches the mean life-time of neutrons in the detector. To overcome this limitation, a special high intensity "flare" monitor has been designed (see Appendix D). This is in essence a smaller version of the LMSC monitor, but with a sensitivity and characteristic neutron mean-life such as to enable it to resolve multiplicity spectra under the very high flux conditions which exist at high altitudes and during major cosmic ray flares. This flare monitor when completed will be employed in high altitude latitude survey experiments and on a longer term basis will be used to augment the operation of the large multiplicity monitor on White Mountain during the coming active sun years.

X   MONITOR CALIBRATION

At each monitor servicing, i.e., approximately every **two** weeks, calibration runs were made with RaBe source neutrons. The total counting rates, as well as the individual counter rates, were determined. Also, the pulse height distributions and discriminator levels were checked for each of the **26** counter, amplifier, and discriminator channels. Throughout the period of operation, no discernible drifts have been detected in any of these rates, levels or distributions. The electronic master clock was periodically synchronized with WWV time signals.

XI   OPERATIONAL **SUMMARY**

For the first month of the contract period, which began June 22, 1965, the monitor was operated in LMSC Building 202 in Palo Alto. During this

time, operation was continuous except for brief intervals when servicing, calibrations or modifications were in progress. July 2, 1965, marked the beginning of the relocation to a trailer van and July 30 the first operation in the van at Palo Alto. On August 6, 1965, the van was started on its way to the University of California's Barcroft Laboratory on White Mountain. By August 17th, the monitor was operating at the new site. The equipment survived the move without damage.

From the beginning difficulty was experienced with A. C. power at the mountain location. Barcroft is situated at 3800 meter elevation a few miles south of the 4350 meter summit of White Mountain. The power line which originates at Bishop, California, runs up Silver Canyon to its head and then follows the ridge of the Indo-White Mountain range for about 12 miles to the laboratory site. Most of the power problems are attributable to a combination of factors including the length of the line, its exposed location and the prevailing severe climatic conditions. A major portion of the difficulties encountered during the ten months of Barcroft operation were due to power problems. A secondary source of difficulty was the perforated paper tape data recording system. However, failure of this system was generally only an inconvenience, as the same information was also recorded in parallel on a data printer. Aside from the above mentioned difficulties, the monitor operated with a gratifying degree of reliability. This characteristic of dependability is necessary to the monitor's unattended mode of operation. Data was successfully obtained for about 75 percent of the time at Barcroft. This percentage is expected to increase dramatically with the completion of the

planned conversion of the monitor to battery operation with a standby auxiliary motor generator for battery charging in the event of power failure. Because of the greater interest of the high counting rate mountain data, it was decided to continue monitor operation at Barcroft rather than returning it to Palo Alto as originally planned. Experience has shown that the logistics of maintaining the station on the mountain, even during the winter months, are not insurmountable.

The photograph, Fig. **24,** shows the monitor van at Barcroft in February 1966. Electric heating tapes were installed on the roof of the van over the detector area to prevent the accumulation of snow during quiet wind conditions. Normally the wind kept the roof clear and also scoured the snow from beneath the van. The photograph shows the guy cables attached to the upper corners of the trailer and the mast-mounted vaned pitot tube.

XII PUBLICATIONS

The abstract of a paper presented at the 47th annual meeting of the American Geophysical Union is included below. A paper to be submitted for publication in the Journal of Geophysical Research is in final stages of preparation. This paper reports the results of an analysis of the operation of the LMSC multiplicity monitor to date. Pre-prints will be supplied the National Aeronautics and Space Administration as soon as they are available.

Abstract

Neutron Multiplicity Monitor Observations of Secondary Cosmic Radiation at Sea Level and 3800 Meter Elevation in 1965

R. A. Nobles, L. L. Newkirk and M. Walt
(Lockheed Palo Alto Research Laboratories, Palo Alto, California)
E. B. Hughes
(Princeton University, Princeton, New Jersey)

Fig. **24**   The monitor van at Barcroft Laboratory site, February **1966.**

Neutron multiplicity spectra observed by the Lockheed monitor at sea level (Palo Alto) and 3800 meter elevation (White Mountain, Calif.) are fitted with computed spectra using known monitor characteristics and trail energy spectra for the nucleonic component of the secondary radiation. A power law energy distribution of the form $N(E) \sim E^{-\eta}$, E in Bev, with $\eta = 2.22$ and 2.03 for sea level and 3800 meter elevation respectively, are found to give a good fit to the data. Typical hourly counting rates are given in the following table:

	Total/Hr	m = 1	2	3	4	5	6	7	8
3800M	580000	193000	56900	24500	12000	6350	3580	2200	1450
Sea Level	33000	15800	3190	1250	568	276	147	89	54
Ratio 3800M/S. L.	17.6	12.2	17.8	19.6	21.2	23.0	24.4	24.7	27.2

The barometric absorption coefficient for multiplicity channel m = 1 at sea level was found to be significantly less than those for higher channels, a feature satisfactorily explained in terms of a —10 percent contribution to the counting rate of this channel by μ -mesons, which compared to nucleons have a longer interaction mean free path and produce neutrons with a lower mean multiplicity. After allowance is made for this effect the barometric absorption coefficients are independent of multiplicity and altitude, within the accuracy of the measurements, indicating an energy insensitivity of the nucleon-nucleus interaction cross-sections in the range studied.

XIII ACKNOWLEDGEMENT

XIV   REFERENCES

Bachelet, Balata, Dyring and Iucci (1965); Nuovo Cimento 35, 23.

Blackman and Tukey (1959), Measurement of Power Spectra, from the Point of View of Communications Engineering.   Dover Publications, New York.

Carmichael, H. (1962), Space Sci. Rev. 1, 28.

Carmichael, H. (1964a), IQSY Instruction Manual #7.   IQSY Secretariat, 6 Cornwall Terrace, London, N. W. 1, England.   AECL - 1885.

Carmichael, H. (1964b), Private Communication.

Cocconi, Tongiorgi and Widgoff (1950), Phys. Rev., 79, 768.

Falconer, R. E. (1947), Trans. Amer. Geophys. Union, 28, 385.

Geiger, K. W. (1956), Canad. J. Phys., 34, 288.

Griffiths, Hatton, Ryder and Harman (1966), J. Geophys. Res. 71, 1895.

Hughes, E. B. (1961), Ph.D. Thesis, University of Leeds, Leeds, England.

Hughes, Marsden, Brooke, Meyer and Wolfendale (1964), Proc. Phys. Soc. 83, 239.

Lapointa and Rose (1962), Canad. J. Phys. 40, 687.

Lindgren, S. (1966), Private Communication.

Lockwood, J. A. (1962), Am. J. Phys., 30, 10.

McCracken, K. G. (1962), J. Geophys. Res. 67, 423, 435.

Pomerantz, Sandstrom and Rose (1958), Nuovo Cimento, Sup. VIII, 257.

Sandstrom, Pomerantz and Grönkvist (1963), Tellus XV, 184.

Simpson, Fonger and Treiman (1953), Phys. Revs. 90, 934.

Simpson, J. A. (1964), Pontificia Academia Scientravum Scripta Varia. , 25, 324 (Rome).   A64-15859.

Webber, W. R. (1962), Progress in Elementary Particle and Cosmic Ray Physics, VI, Chapter II, North Holland Publishing Company, Amsterdam.

XV   APPENDIX A

   Monitor Description: The monitor shown in cross-section in Figs. 25 and 26 has a bismuth target in the form of a pseudo-cylindrical segment approximately 16 inches in diameter and 16 inches long.   This target is surrounded by an 8-inch thick layer of 4 x 4 inch graphite logs in which are embedded twenty-six BF_3 neutron proportional counters.   The graphite is in turn enclosed by a 3-inch thick paraffin wax reflector.   To reduce the background from externally produced neutrons the reflector is surrounded by a layer of cadmium and finally a 4-inch thick paraffin and plywood shield.   The monitor assembly has the form of a 1.25 meter cube of 2000 kg weight, of which   810 kg is bismuth,   740 kg graphite, $\sim$ 360 kg paraffin and 53 kg cadmium.   Doors on opposing sides of the cube give access to the counter tubes and their preamplifiers and wiring networks. A grid of holes in the bismuth target and a test hole in one side of the cube provide for the insertion of a Ra-Be neutron source for efficiency measurements and routine counting rate checks.   *

   The moderator is composed of reactor-grade graphite, a high purity material produced especially for nuclear applications.

   The counters, manufactured by Reuter-Stokes Inc. , Cleveland, Ohio, have a 2-inch diameter stainless steel body with a 0.002 inch diameter

Note:

   *Carmichael (1964B) has reported unstable operation of a graphite moderated neutron monitor which is probably attributable to the hygroscopic action of trace impurities.   The present monitor exhibits no such instability within the statistical accuracy of observed counting rates.

Fig. 25   Diagram of the LMSC multiplicity monitor in vertical **cross-**
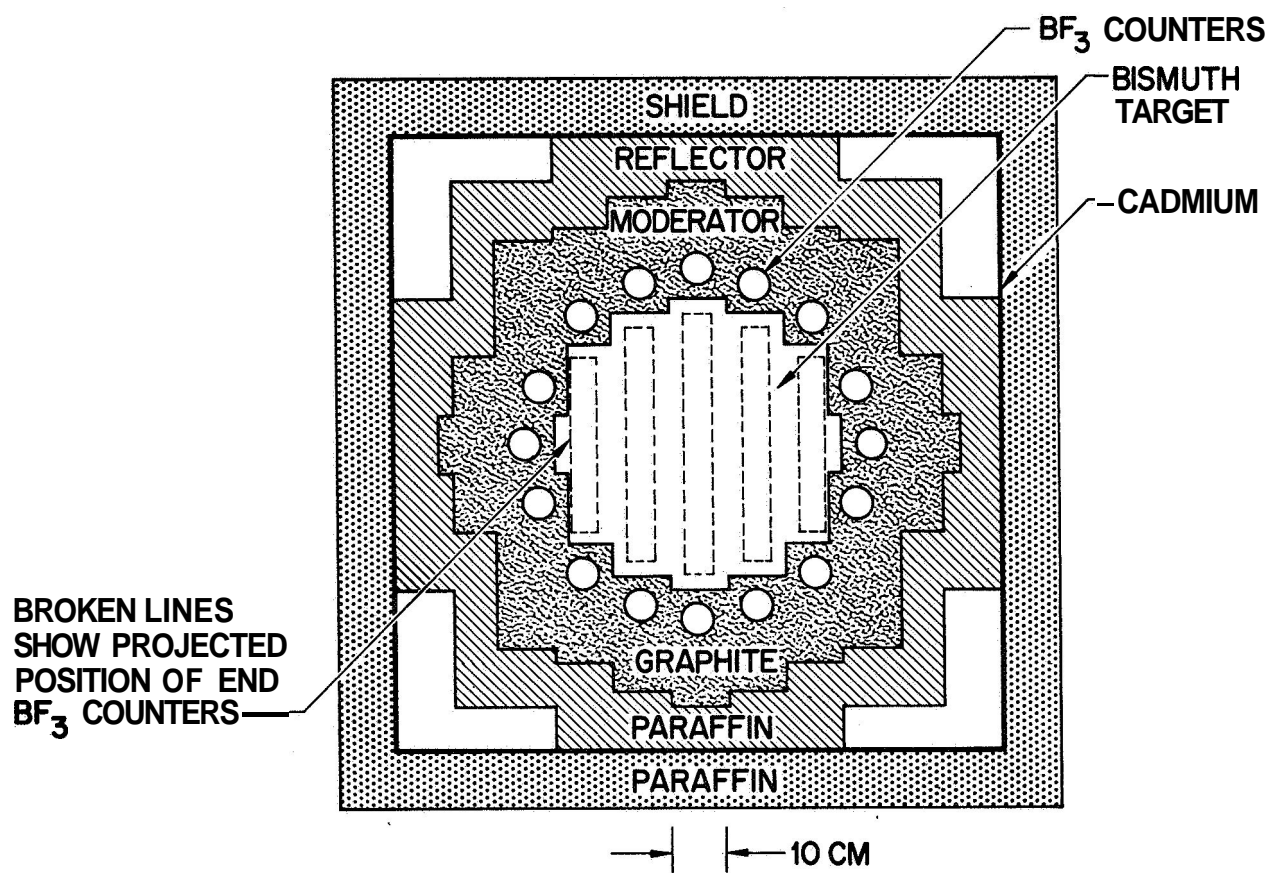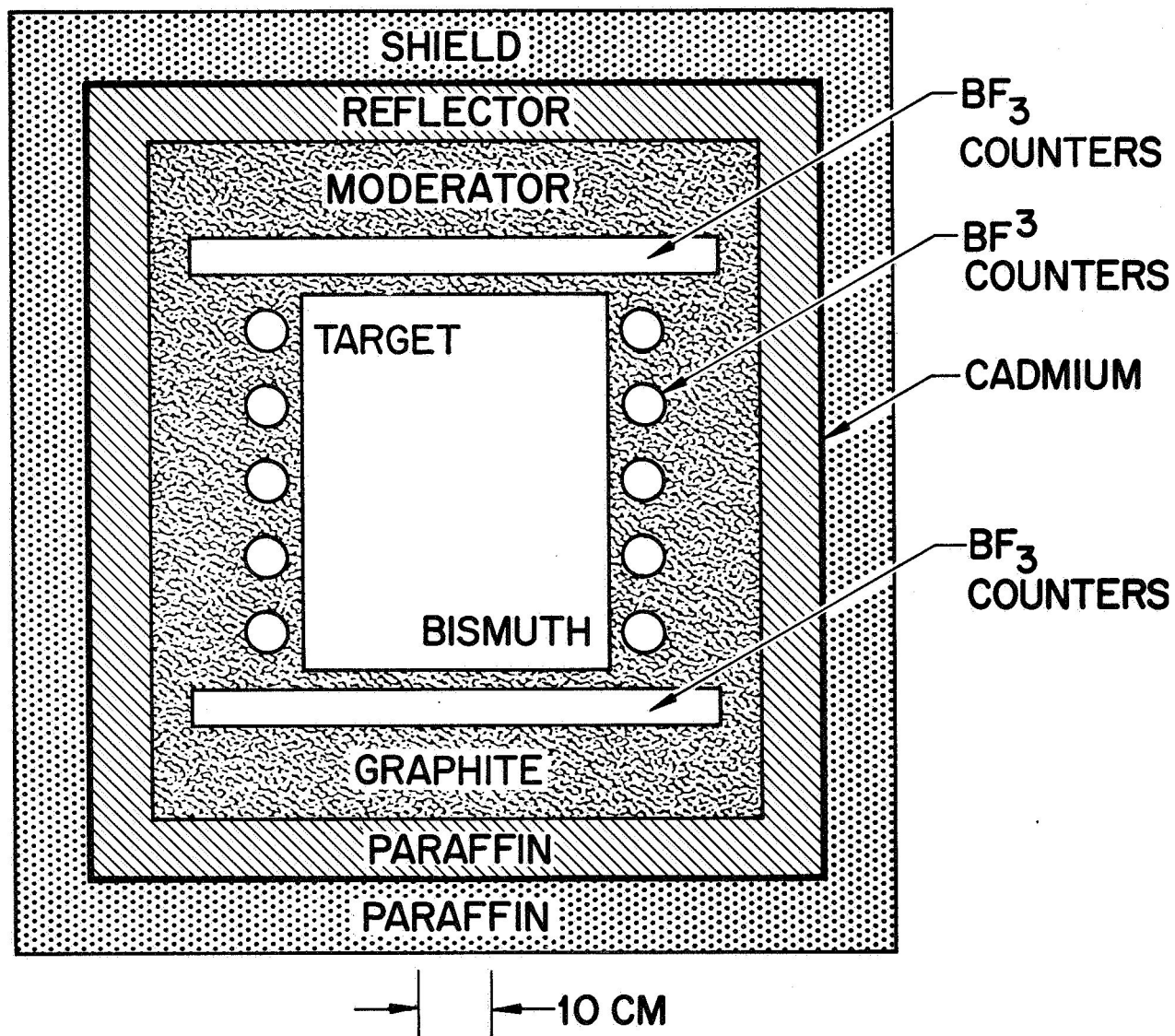
     section.

BF₃ COUNTERS

BISMUTH TARGET

CADMIUM

SHIELD

REFLECTOR

MODERATOR

BROKEN LINES SHOW PROJECTED POSITION OF END BF₃ COUNTERS

GRAPHITE

PARAFFIN

PARAFFIN

10 CM

Fig. *26*   Cross-section diagram of monitor in the horizontal symmetry

plane.

tungsten wire anode, alumina insulators, are of all welded and brazed construction, and are filled to **70 cm** Hg pressure with purified 96% B_{10} **en**riched BF_3 gas.   Operating at ~ **3200** volts with grounded cathodes they give essentially no spurious breakdown pulses and exhibit pulse height distributions which vary only a few percent between tubes of equal length.   Fig. **27** shows the complete monitor together with its electronics equipment racks.   An end view of the monitor is shown in Fig. 28 and in Fig. 29 the door has been removed showing the plywood-incased paraffin reflector and the voltage and signal distribution networks for five vertical counters.   The opposite end is similar except that 16 horizontal counters are served in addition to the five vertical counters.   Fig. 30 is a view with the reflector removed, showing the graphite moderator and the counter electronic units.

Electronics: Each counter has a unitized transistor preamplifier, high voltage filter and signal decoupling network.   Fig. 31 shows a typical counter tube-electronics unit and Fig. **32** shows an exploded view of the assembly. Each preamplifier is connected to an individual transistorized amplifier, discriminator and pulse forming circuit.   The paired pulse resolving time of any one counter channel is about **7** psec and between different channels about 0.1 μ sec.   The counter channels are divided into two symmetrically located banks of 13 detectors each; signals in each bank are fed into a gated digital scaler' (scalers I and 11).   The ratio of the counts in the **two** banks gives a running check on instrumental consistency.   The signals from the two banks are combined and fed into the address scaler of a standard R. I. D. L. 400-channel transistorized pulse height analyzer and also into a gate generator.   The first

Fig. 27   Photograph showing front half of monitor cube and the elec-
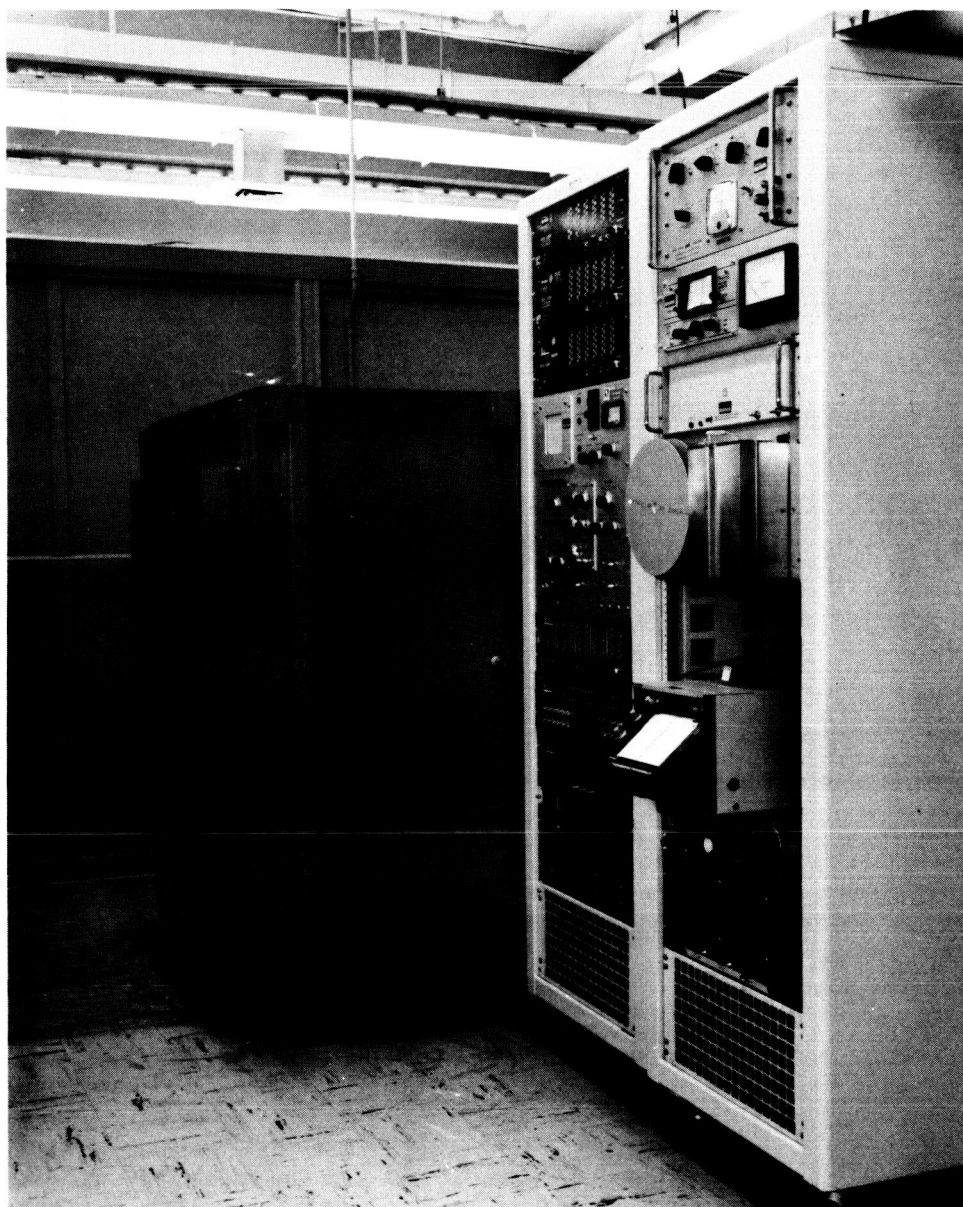
tronics equipment racks.

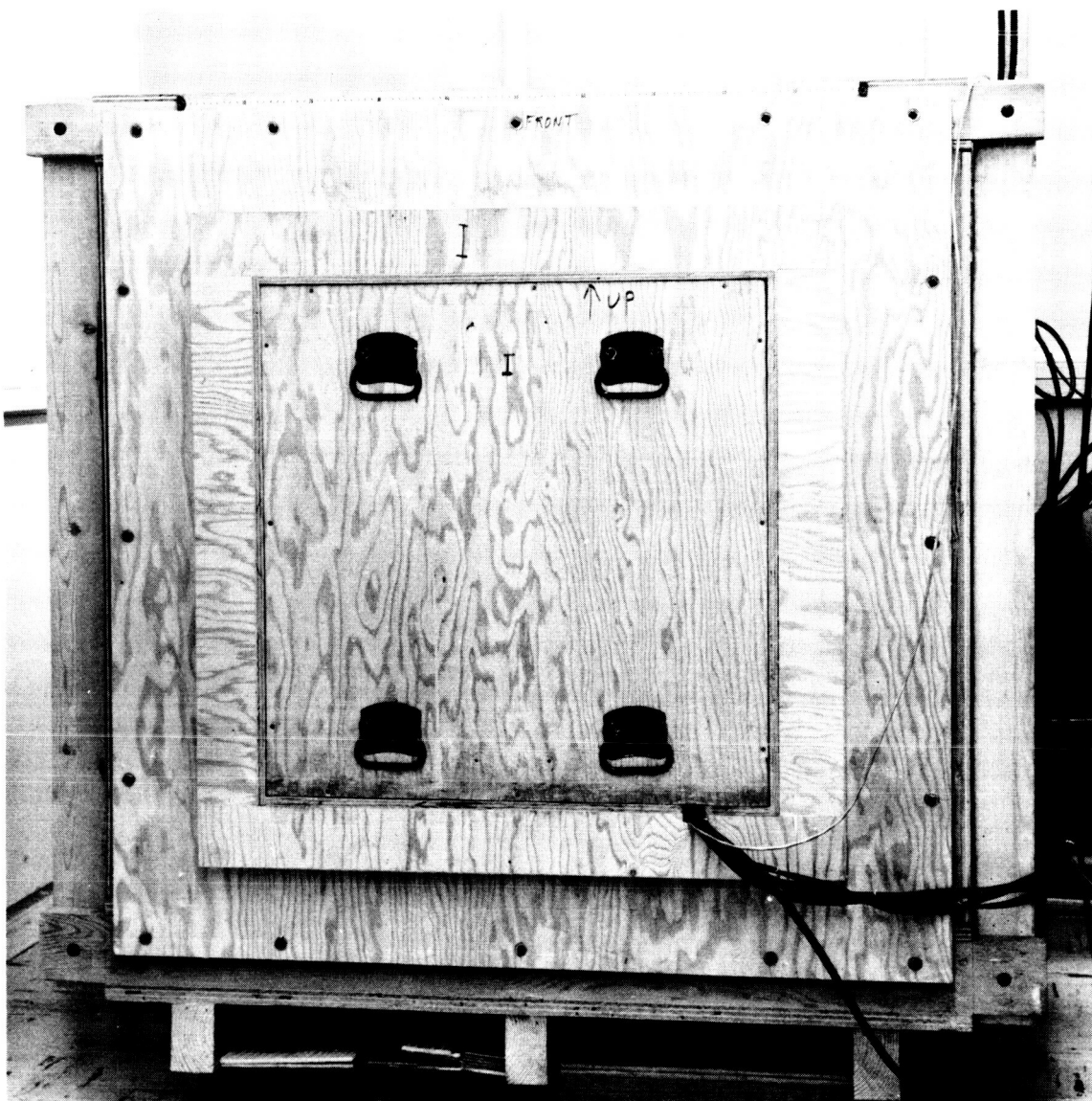Fig. 28   End **view** of monitor **cube.**

Fig. 29   Monitor with door removed, showing plywood-encased reflector and voltage and signal distribution networks for five vertical counters.
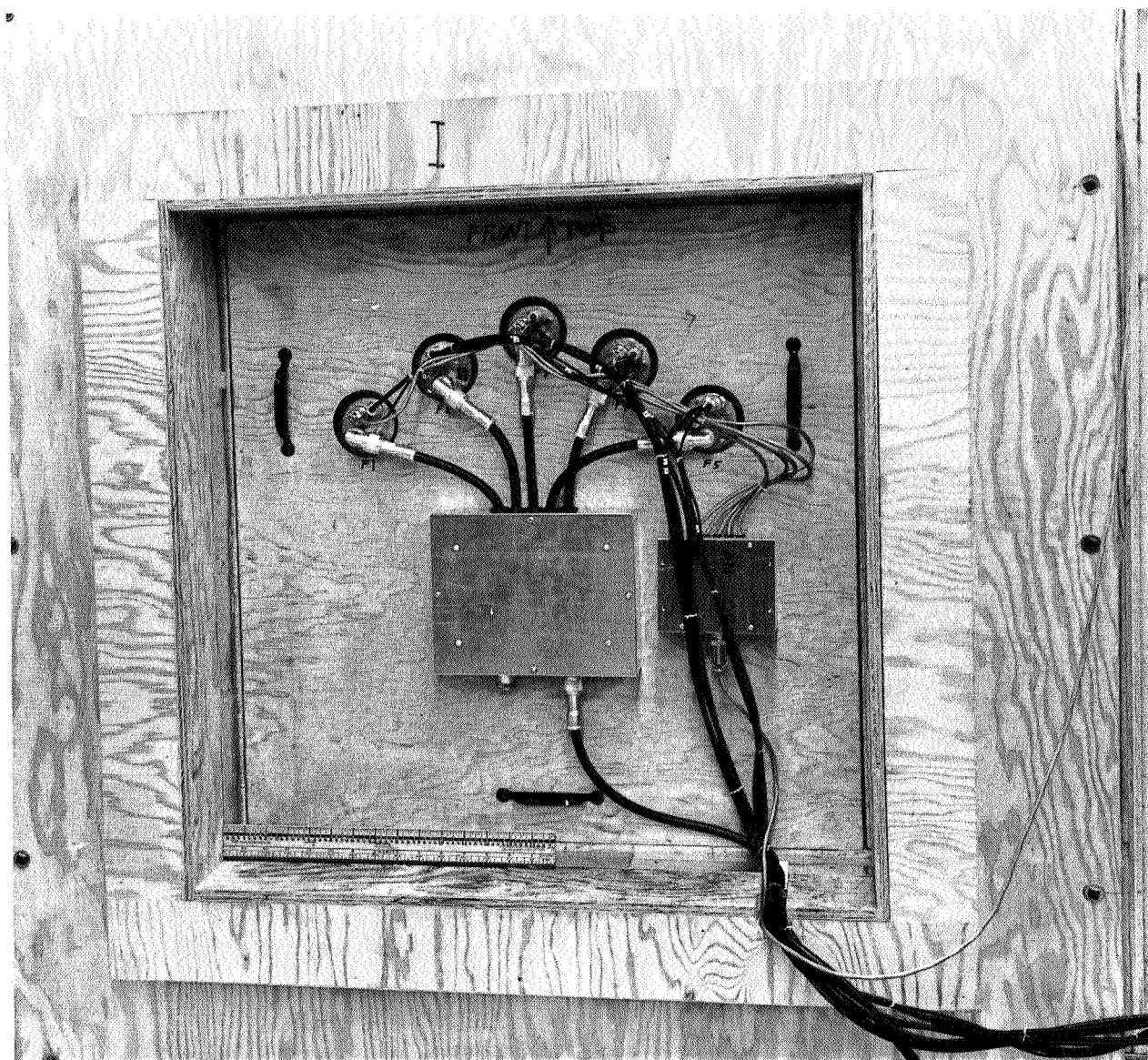
Fig. 30   Monitor with reflector removed showing graphite moderator and counter electronics units.

Top

a
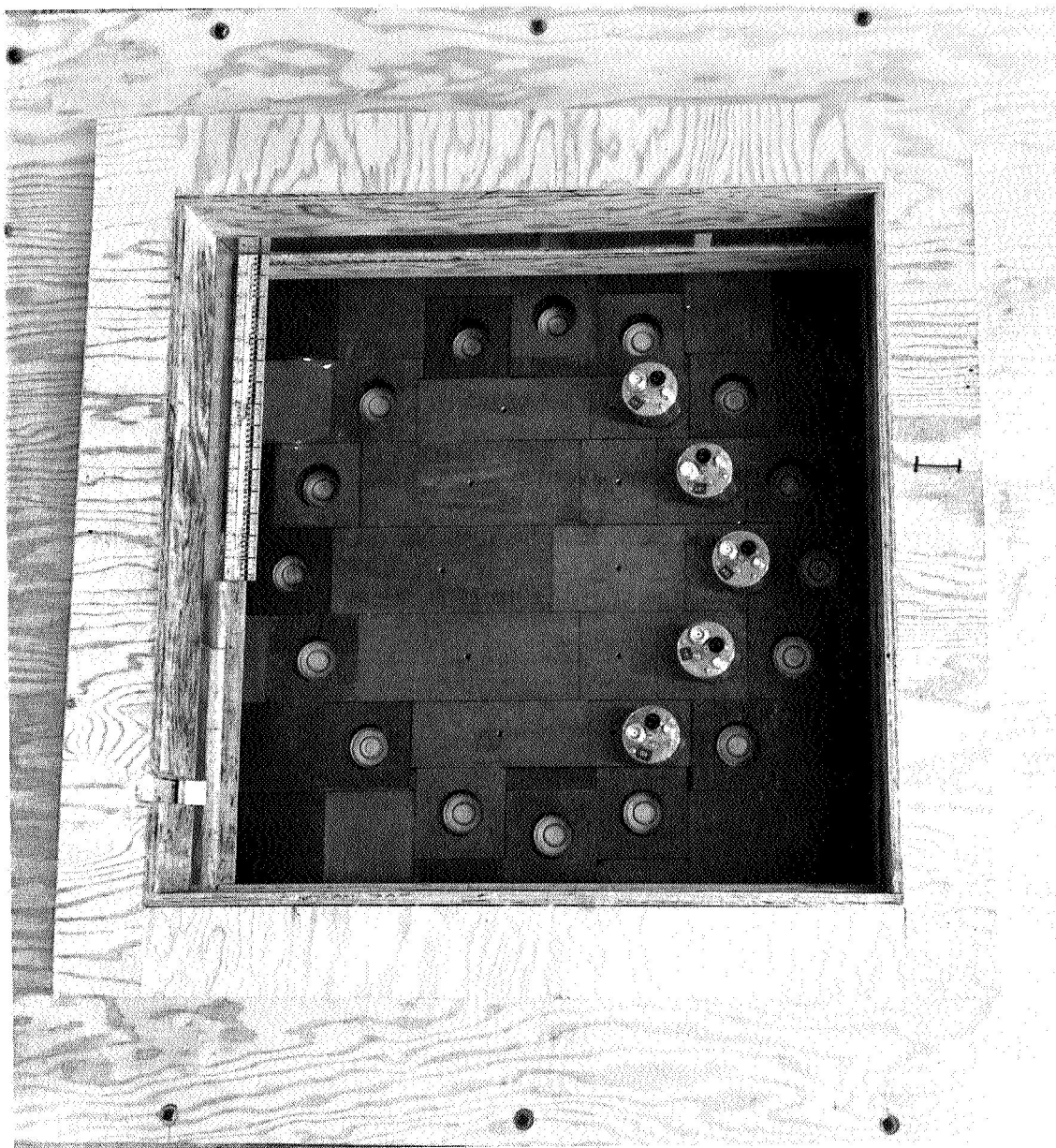
Fig. 31   A typical counter tube-electronics unit. All counters and electronics units are interchangeable. The mating of the counter tube and electronics unit is by a simple threaded assembly.

Fig. 32   An exploded view of a counter assembly. A sample preamplified

is shown in the foreground.   The functional preamplifier is not

visible in the photograph.

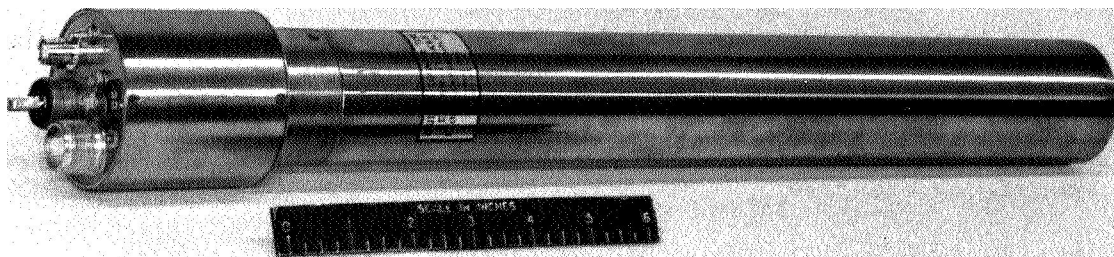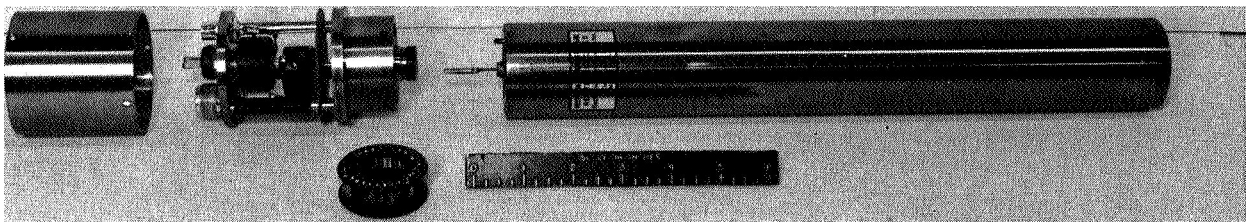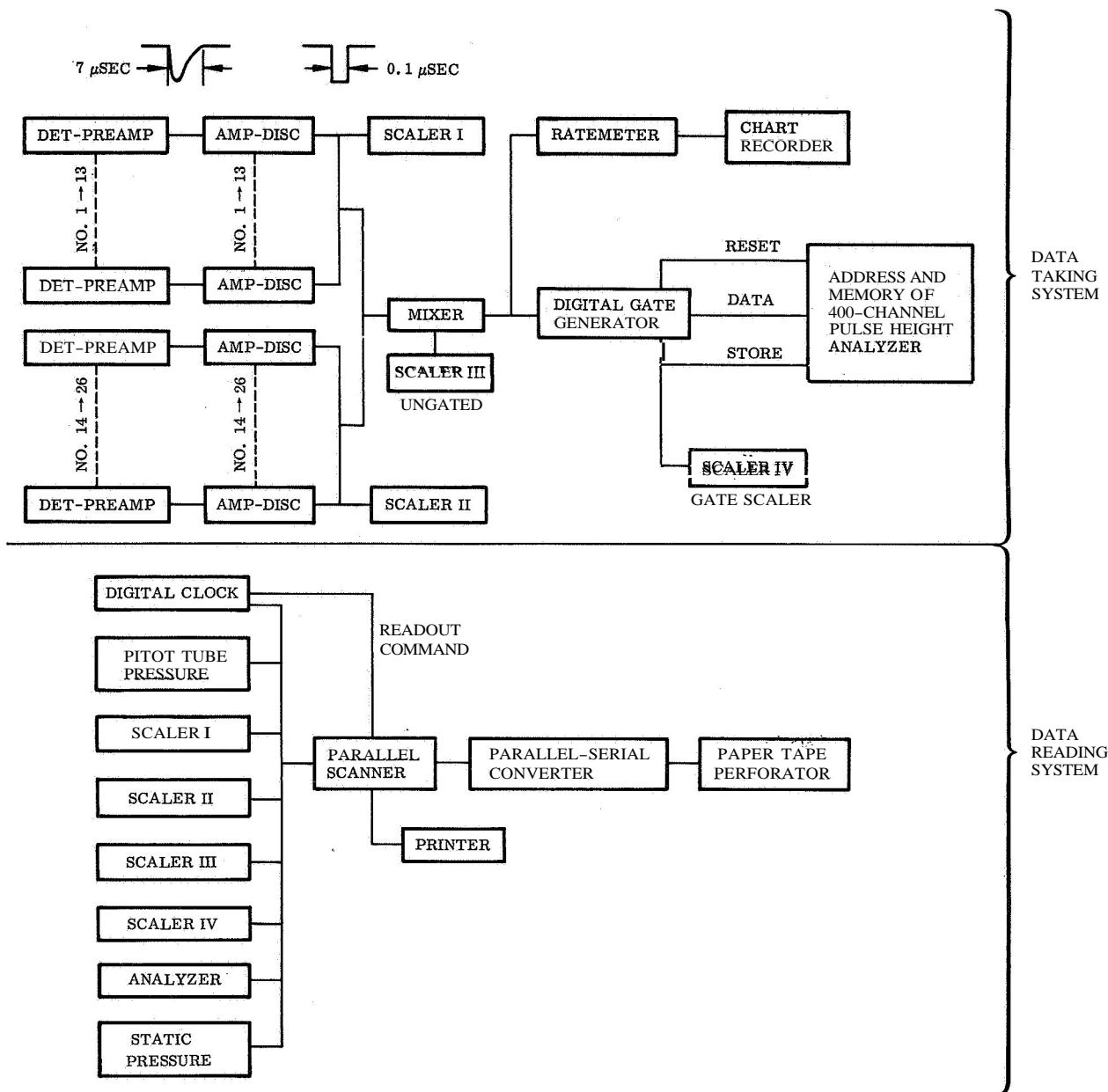pulse of an event gates on the address scaler for a time interval commensurate with the mean life of neutrons in the monitor. At the end of the gate interval the address scaler count is transferred to the analyzer memory and the scaler cleared and reset to await the next event. This procedure sorts each event according to the neutron counts contained, i. e. , according to observed multiplicity. Scaler **IV** records the total number of gates generated, and scaler **III** , which is ungated, records the total number of neutrons detected. Also recorded is the atmospheric pressure to the nearest 0.01 milli-bar as measured by a fused quartz burden tube precision pressure gauge,[*] and the time and date of the readout. Two barometric pressures are recorded, the static pressure at the monitor and the dynamic pressure from a mast-mounted windward vaned pitot tube. The pitot pressure is used in data correction because pressure so measured partially compensates for the pressure deficiency produced by the airflow over the mountain location and hence gives a better indication of the air-mass over the monitor than that deduced from the static pressure (Falconer, 1947). Since the monitor is not detecting neutrons during readout, the time interval required for the process is recorded and the observed rates ,adjusted accordingly. The average time required for a mountain elevation readout is about 19 seconds.

Fig. **33** shows a block diagram of the complete electronic system. Readout commands are provided at pre-selected fixed times by the digital clock. Data are recorded on **two** parallel, redundant systems: on perforated paper tape and by a data printer. An analog count rate meter operating off the gate count drives a stip-chart recorder to provide a visual record of the gate counting rate.

[*] Manufactured by Texas Instruments *Co.,* Model #141

Fig. **33**   **A block diagram of the electronic system.**

7 μSEC —— 0.1 μSEC

DET-PREAMP — AMP-DISC — SCALER I — RATEMETER — CHART RECORDER

NO. 1 → 13

DET-PREAMP — AMP-DISC

MIXER — DIGITAL GATE GENERATOR — RESET / DATA / STORE — ADDRESS AND MEMORY OF 400–CHANNEL PULSE HEIGHT ANALYZER

SCALER III
UNGATED

DET-PREAMP — AMP-DISC

NO. 14 → 26

DET-PREAMP — AMP-DISC — SCALER II

SCALER IV
GATE SCALER

DATA TAKING SYSTEM

DIGITAL CLOCK

READOUT COMMAND

PITOT TUBE PRESSURE

SCALER I

PARALLEL SCANNER — PARALLEL–SERIAL CONVERTER — PAPER TAPE PERFORATOR

SCALER II

SCALER III

PRINTER

SCALER IV

ANALYZER

STATIC PRESSURE

DATA READING SYSTEM

XV APPENDIX B

Overlap and Deadtime Corrections: When the counting rate is such that there is a significant probability of coincidence of two multiplicity events within a single gate period the shape of the observed multiplicity distribution becomes distorted and it is necessary to make an overlap correction. The electronic circuitry is such as to preclude the possibility of a gate being initiated by residual neutrons associated with a preceding gate. Hence events which occur during the deadtime after a gate has closed do not distort the shape of the observed distribution, but serve only to prolong the preceding gate deadtime. The following set of simultaneous equations relate the observed multiplicity rates to the overlap corrected rates. The equations are based on elementary probable considerations in which the small contribution from higher order coincidences are neglected.

$$R_1 = R\,P_1 r_1$$

$$R_2 = R\,P_1 r_2 + R\,P_2 r_1\,(r_1 P_1 1\,t\,r_2 P_2 1\,t\,r_3 P_3 1\,t\ldots)$$

$$R_3 = R\,P_1 r_3\,t\,R\,P_2 r_1\,(r_2 P_2{}^2\,t\,r_3 P_3{}^2\,t\,r_4 P_4{}^2\,t\,\ldots) \tag{4}$$

$$+ R\,P_2 r_2\,(r_1 P_1{}^1 + r_2 P_2{}^1 + r_3 P_3{}^1 + \ldots) \qquad \text{etc.}$$

where R_m is the observed rate of occurrence of multiplicity m events and R is the total rate for gates of all multiplicities. The r_m represent the true probability of a multiplicity event having an observed multiplicity m.

P_1 and P_2 are probability terms defined by the expression,

$$P_1 = P_1{}' + P_2{}'\,P$$

$$P_2 = P_2{}'\,(1-P) \tag{5}$$

where P_1' is the Poisson probability that a new multiplicity event will not occur within a time (τ + d) following the previous event which initiates a detector gate. Here, τ is the gate length and d the observed average dead-time. P_2' is the Poisson probability that a second event will occur within the time (τ + d) of the first event. Since higher order coincidences are neglected, P_1' and P_2' must sum to the value one. P_2' was therefore determined from the relationship

$$P_2' = 1 - P_1' \tag{6}$$

The quantity P is the Poisson probability that a second neutron multiplicity event that has occurred will fall within the time τ to (τ + d). Values for the Poisson probabilities P_1', P_2', and P were determined by calculation. The actual gate rate, R_t, required in making these calculations was obtained from the observed gate rate, R, by the use of the well known equation for making counter deadtime corrections,

$$R_t = \frac{R}{1 - R(\tau + d)} \tag{7}$$

The term p_m^{ℓ} in Equation (4) represents the binomial probability that ℓ of m neutrons from a second multiplicity event that has occurred within the gate generated by the first event will be detected.

$$p_m^{\ell} = \binom{m-1}{\ell-1} \bar{\epsilon}^{\ell-1} (1-\bar{\epsilon})^{m-\ell} \tag{8}$$

In Equation (8), $\bar{\epsilon}$ is the average probability under the stated conditions that a single neutron will be detected. The value of $\bar{\epsilon}$ was calculated using the experimentally measured distribution of total counting rate as a function of gate length.

In solving Equations **(4)** for the r_m they were first truncated at some maximum multiplicity, then inverted and the r_m determined by an iteration procedure.   The equations were found to be stable and to converge after only a few iterations.   The r_m, when multiplied by R_t, give the corrected multiplicity rates sought.   The magnitude of the correction up to m = **20** can be seen in Table 1.

XV APPENDIX C

<u>Monitor Statistics:</u>   If N_m is the rate of observing events of multiplicity m, U is the total rate and g is the gate rate, then

$$g = N_1 + N_2 + N_3 + \ldots = C N_m$$

$$U = 1 \cdot N_1 + 2 \cdot N_2 + 3 \cdot N_3 + \ldots = \Sigma m N_m = \overline{m}\, g$$

where $\overline{m} = \dfrac{U}{g}$, the average multiplicity

The variance of U and g are given by

$$\sigma_u = (\Sigma\, m^2\, N_m)^{\frac{1}{2}} = K\, U^{\frac{1}{2}}$$

and

$$\sigma_g = (C\, N_m)^{\frac{1}{2}} = g^{\frac{1}{2}} .$$

The ratio of the relative statistical accuracy of U and g is given by

$$R = \frac{\sigma_u/U}{\sigma_g/g} = \frac{K(\overline{m}g)^{\frac{1}{2}}/mg}{g^{\frac{1}{2}}/g} = \frac{K}{\overline{m}^{\frac{1}{2}}} .$$

Values for $\overline{m}$, K and R for typical sea level mountain data are given in the following table.

Table III

|	$\overline{m}$	K	R
Sea Level	1.63	2.00	1.57
3800 Meter Elevation	1.90	2.30	1.67

Thus, the gate g is determined with higher statistical accuracy than the numerically greater total count rate, U.

XV APPENDIX D

Cosmic Ray Flare Neutron Multiplicity Monitor: The LMSC neutron multiplicity monitor, now operating on White Mountain, is limited in its ability to respond to major cosmic ray flare events.   This is due to the long mean life of neutrons in the monitor and the long gate lengths which this necessitates, and also to a rate dependent deadtime feature, whose purpose is to minimize accidental overlap of individual events.   These inherent and necessary characteristics lead to the generation of excessive deadtime and eventually to a complete jamming of the monitor should the counting rate increase by several hundred percent over the ambient White Mountain rate. For example, the existing monitor would have been totally dead during the great cosmic ray flares of the last solar cycle, as these events gave neutron intensities of 1000 to 2000 percent over preflare values.   The proposed flare monitor would be able to resolve the intensity and energy variations during such events.

In essence the new monitor, see Figs. 34 and 35, will be a small version of the existing multiplicity monitor, except that the target and moderator will be lead and paraffin instead of bismuth and graphite.   The choice of these

Fig. **34**   **A transverse cross-section view of the LMSC flare** monitor.

LEAD

COUNTERS

PARAFFIN

CADMIUM
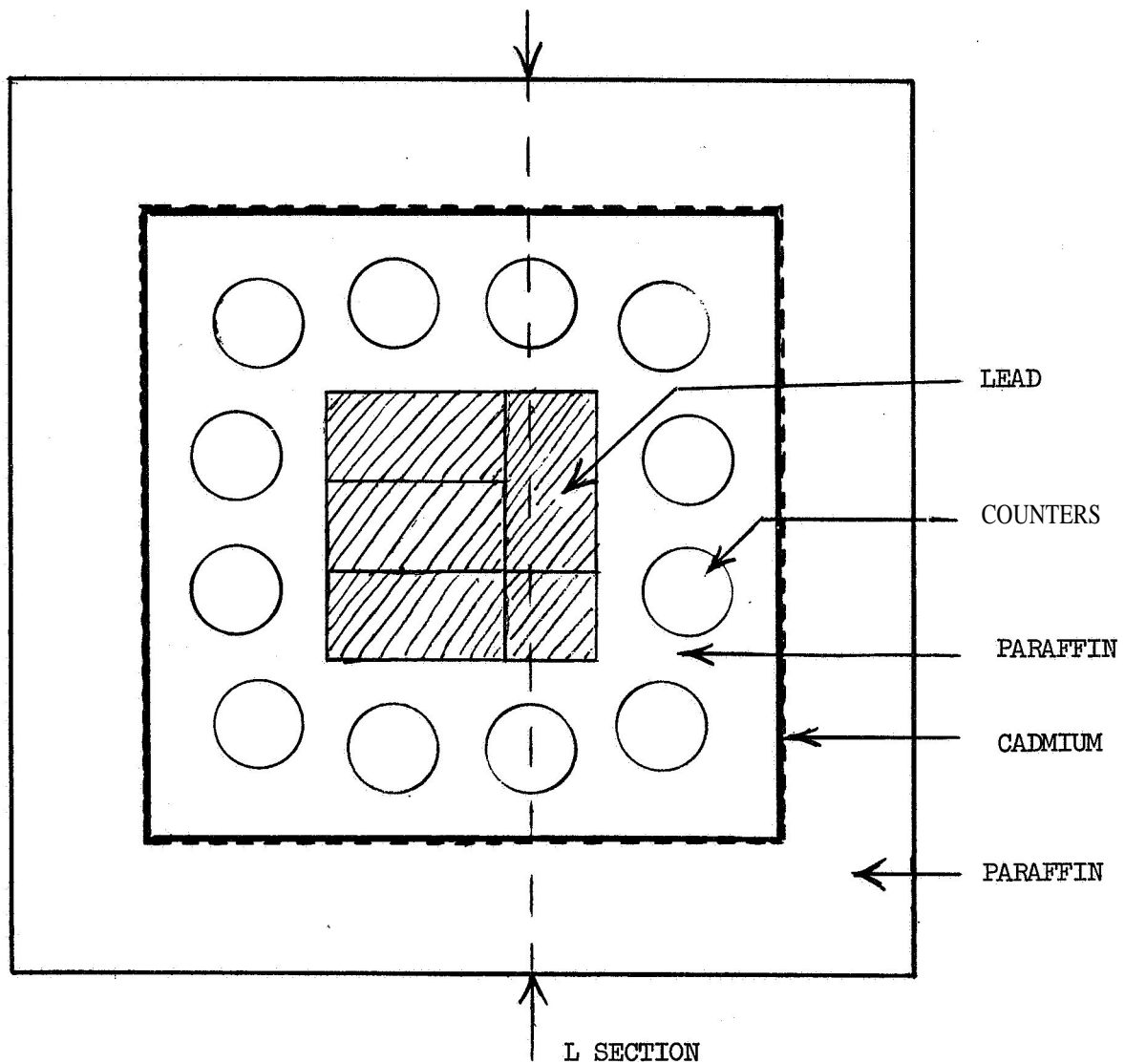
PARAFFIN

L SECTION

TRANSVERSE CROSS SECTION VIEW

SCALE: 1/4   (Preliminary)
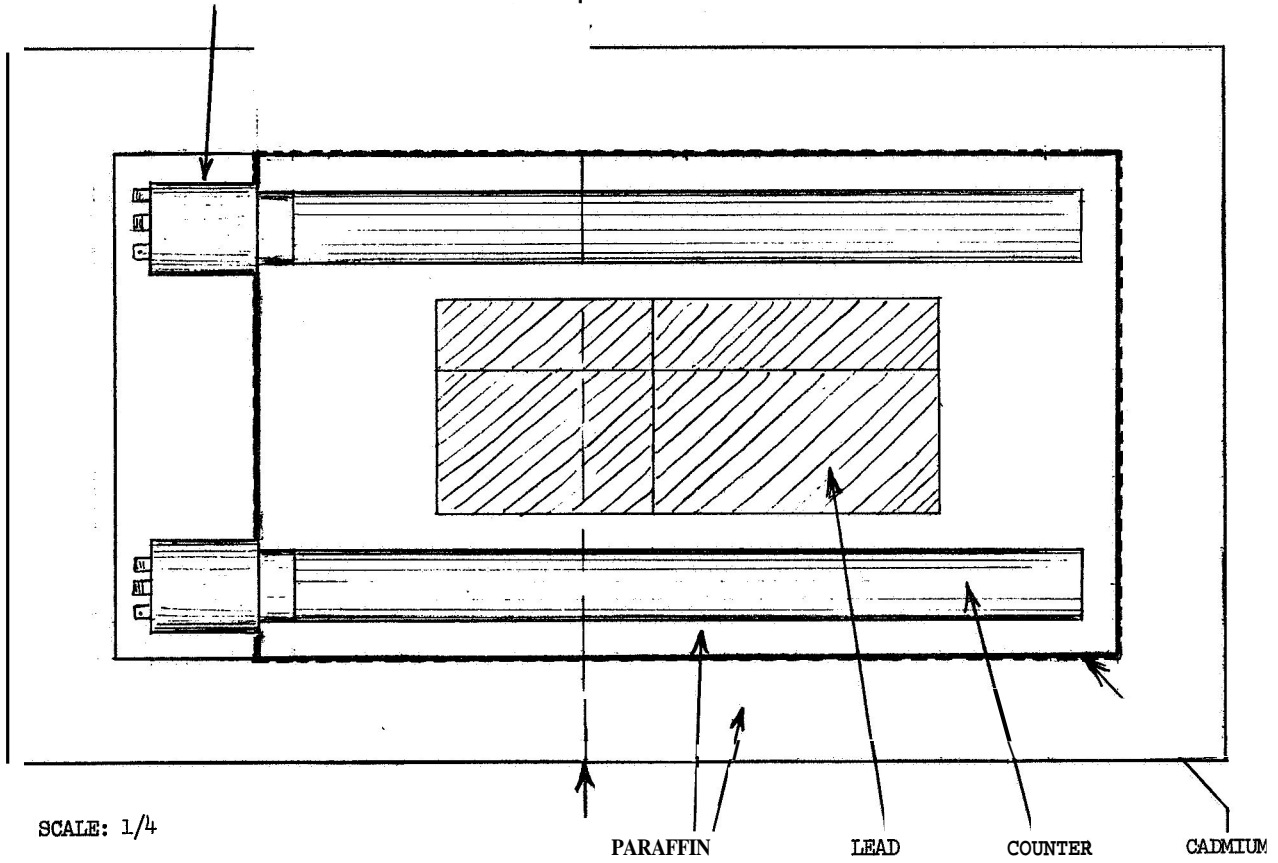
Fig. **35**   Longitudinal cross-section view of the LMSC flare monitor.

LONGITUDINAL CROSS SECTION VIEW

PREAMPLIFIER   T SECTION   (Preliminary)

SCALE: 1/4

PARAFFIN   LEAD   COUNTER   CADMIUM

materials leads to a somewhat reduced counting efficiency but gives a shorter neutron mean life and thus allows the use of shorter gate lengths. A relatively large counting volume, provided by twelve 2" diameter x 20" long BF_3 tubes, tends to counteract the reduced efficiency caused by the use of lead and paraffin and also contributes to reducing the neutron mean life. Electronics will be similar to that of the large monitor but simplified and improved as is to be expected from a second generation design.

Table IV gives a comparison of some of the characteristics of the proposed flare monitor and the existing LMSC multiplicity monitor.

The lower counting rate and shorter neutron mean life in the flare monitor will allow handling of cosmic ray intensities at least 20 times that of the large monitor without excessive counting losses. It is expected that the new monitor will operate continuously in conjunction with the existing monitor and during major flare events will assume the role of prime observing instrument.

Installation will be in the existing trailer van, and some of the electronic circuitry and auxiliary equipment can be shared by the two monitors. However, the basic design will be such as to be readily adaptable to independent operation for special applications.

Table IV

	Flare Monitor	LMSC Multiplicity Monitor
Producer (Target)	90 Kg Pb	810 Kg Bi
Moderator	10 cm Paraffin	20.4 cm Graphite
Reflector	---	7.6 cm Paraffin
Shield	7.5 cm Paraffin 0.08 cm Cd.	7.5 cm Paraffin 0.08 cm Cd.
Number of Counters	12	26
Counter Filling	70 cm Hg BF_3 96 percent B^{10} enriched	same
Total Counting Volume	12.4 Liters	29.8 Liters
Total Monitor Weight	$\approx$ 245 Kgm	$\approx$ 2000 Kgm
Overall Dimensions	.51 M x .51 M	1.34 M x 1.34 M by 1.28 M
Estimated Relative Counting Rate	0.1	1.0
Neutron Mean Life	200 psec (estimated)	400 μsec